Physics of the Dark Universe 47 (2025) 101777

Contents lists available at ScienceDirect

Physics of the Dark Universe

journal homepage: www.elsevier.com/locate/dark

Full length article

Construction of wormhole under embedded approach through dark matter halos in $F(T, T_G)$ gravity

Asifa Ashraf [a,b], Wen-Xiu Ma [a,c,d,*], Faisal Javed [e], S.K. Maurya [f,**], Farruh Atamurotov [g,h,i], Abdelmalek Bouzenada [j], Magda Abd El-Rahman [k]

[a] School of Mathematical Sciences, Zhejiang Normal University, Jinhua Zhejiang, 321004, China
[b] Research Center of Astrophysics and Cosmology, Khazar University, Baku, AZ 1096, 41 Mehseti Street, Azerbaijan
[c] Department of Mathematics and Statistics, University of South Florida, Tampa, FL 33620-5700, USA
[d] School of Mathematical and Statistical Sciences, North-West University, Mafikeng Campus, Private Bag X2046, Mmabatho 2735, South Africa
[e] Department of Physics, Zhejiang Normal University, Jinhua 321004, China
[f] Department of Mathematical and Physical Sciences, College of Arts and Sciences, University of Nizwa, Nizwa 616, Sultanate of Oman
[g] New Uzbekistan University, Movarounnahr Str. 1, Tashkent 100000, Uzbekistan
[h] University of Tashkent for Applied Sciences, Str. Gavhar 1, Tashkent 100149, Uzbekistan
[i] Urgench State University, Kh. Alimdjan str. 14, Urgench 220100, Uzbekistan
[j] Laboratory of Theoretical and Applied Physics, Echahid Cheikh Larbi Tebessi University 12001, Algeria
[k] Department of Physics, College of Science, King Khalid University, Abha 61413, Saudi Arabia

ARTICLE INFO

Keywords:
$F(T, T_G)$ gravity
Wormhole solutions
Energy conditions
Dark matter halos
Generalized embedded solutions

ABSTRACT

In this study, we explore generalized Ellis–Bronnikov and embedded wormhole solutions within the context of $F(T, T_G)$ gravity with an anisotropic matter source. To achieve the necessary conditions for wormhole formation, we investigate the energy conditions within $F(T, T_G)$ gravity. Our analysis includes various matter distributions, particularly dark matter halos, using observational data from the $M87$ galaxy. We also explore the results in the framework of $F(T, T_G)$ gravity, considering three different dark matter halo distributions. For each case, the violation of energy conditions proves the presence of strange matter, say exotic matter, which is a necessary condition for wormhole existence in this gravitational model when dark matter halos are present. We investigate the effect of physical parameters on the stable configurations of the generated thin-shell surrounding the wormhole structure. In the first scenario, we can see that the shape function parameters have a significant impact on the shell's stable regions. In addition, the considered black hole contributes significantly to the shell's stability.

1. Introduction

In the mathematical theory of general relativity, there are geometric shapes with imaginary topological configurations that can aid in star travel. Theoretically, wormholes (WHs) connect distant locations in the universe, shortening travel distances and times. Flamm [1] is known for inventing the term "wormhole" and characterized the Schwarzschild-type solution scenario in the application of GR field equations as an inoperative WH. Einstein and others [2] proposed a theoretical relationship called the end model by connecting two identical sections (Schwarzschild Bh), resulting in the creation of a singularity when the wormhole throat collapses. Misner and Wheeler [3] were the original individuals to identify these hypothetical attributes of the GR field equations as WHs. Ellis combined geometry with a scalar field to create a geodesically complete manifold without a horizon, introducing the idea of a traversable wormhole with a topological structure [4]. Bronnikov studied scalar-electrovacuum systems' topologies without scalar charge [5], while Clement described a group of traversable higher-dimensional wormholes [6]. Morris and Thorne suggested the presence of a traversable wormhole linking distant parts of space, with a throat upheld by exotic matter that does not adhere to the null energy requirement (NEC), thus sustaining the wormhole [7]. The question of limiting this problem to WH configuration for physical functions is subject to debate. Extensive studies have been carried out on the

* Corresponding author at: School of Mathematical Sciences, Zhejiang Normal University, Jinhua Zhejiang, 321004, China.
** Corresponding author.
E-mail addresses: asifamustafa3828@gmail.com (A. Ashraf), wma3@usf.edu (W.-X. Ma), faisaljaved.math@gmail.com (F. Javed), sunil@unizwa.edu.om (S.K. Maurya), atamurotov@yahoo.com (F. Atamurotov), abdelmalekbouzenada@gmail.com (A. Bouzenada), majedah@kku.edu.sa (M.A. El-Rahman).

https://doi.org/10.1016/j.dark.2024.101777
Received 28 October 2024; Received in revised form 3 December 2024; Accepted 10 December 2024
Available online 16 December 2024

formation of white holes from the spacetime of black holes and the investigation into their different physical traits [8–10].

According to various cosmological studies [11,12], the rapid expansion of the universe is driven by mysterious dark energy, along with dark matter (DM). Alternative gravity theories are considered promising and contemporary approaches to uncovering the hidden aspects of the universe and understanding its expansion. These theories modify the geometric structure of the Einstein–Hilbert action by incorporating or replacing it with a curvature invariant. To explore alternative gravity theories, we analyzed dark energy, dark matter, and the universe's ongoing expansion. Numerous studies have examined modified gravity theories, adding an extra curvature term to the action [13–23]. Some notable modifications include $f(R)$ gravity, Gauss–Bonnet gravity, $f(R,\mathcal{T})$ gravity, and scalar-tensor theory, among others. Furthermore, significant modifications to the gravitational field equations with fourth-order terms have been achieved by introducing a torsion term T, corresponding to the Gauss–Bonnet term T_G [24,25]. The fascinating characteristics of these gravity theories have drawn the attention of many scientists in modern cosmology, high-energy physics, and astrophysics. Jawad studied the energy conditions of $F(T,T_G)$ gravity in the FRW universe modeled by a perfect fluid, as discussed in [26]. Zubair and Jawad explored thermodynamic equilibrium within the framework of $F(T,T_G)$ gravity [27]. Chattopadhyay et al. [28] investigated potential reconstruction methods in $F(T,T_G)$ gravity by integrating pilgrim dark energy and analyzed the equation of state for various parameters across different scale factors. In his work [29], Keskin examined phantom solutions in $F(T,T_G)$ gravity with different dark energy models. Sharif and Nazir [30] proposed anisotropic models for $F(T,T_G)$ gravity, analyzing various cosmic epochs, including both relativistic and non-relativistic periods.

Numerous approaches to General Relativity (GR) have been developed using various techniques, following Buchdahl's significant modification to gravity theory in 1970: $f(R)$ gravity [31]. This theory alters the Einstein–Hilbert action by incorporating a general function of the Ricci scalar. R. $f(R)$ gravity has been used to explain the geometry related to dark energy models [32,33]. Within this framework, Harko and his team studied stationary spherically symmetric wormholes made of ordinary matter, ensuring compliance with the necessary energy conditions [34]. Rahaman and colleagues proposed new methods for constructing stable wormholes in $f(R)$ gravity, demonstrating that wormhole solutions could exist without requiring exotic matter [35, 36]. In their analysis of the nonexistence theorem for wormhole geometries, Bronnikov and Starobinsky concluded that scalar-tensor models are insufficient to describe wormholes with a positive scalar function [37]. Additionally, Bronnikov and others explored the challenges to the nonexistence of wormholes in $f(R)$ theory, while Bahamonde and colleagues examined wormholes in galactic halos [38,39]. Other studies have focused on static wormholes, with Shamir and Fayyaz investigating traversable wormhole solutions using the Karmarkar condition within $f(R)$ gravity [40].

Böhmmer et al. [41] examined static traversable wormhole (WH) solutions by analyzing a specific $f(T)$ model, along with redshift and shape functions. Their findings demonstrated that physically viable WH solutions can be achieved while meeting energy conditions. Jamil et al. [42] derived exact WH solutions in $f(T)$ gravity for both anisotropic and isotropic cases, investigating energy conditions to explore the properties of the matter involved. Sharif and Shamaila (2015) studied N-C WH solutions in two scenarios. First, they used a viable power-law $f(T)$ model to construct the shape function for WH geometry. They later performed a separate analysis of dynamic and charged WH solutions in the context of $f(T)$ gravity, considering an anisotropic fluid. More recently, Mustafa and his team [43,44] introduced new WH solutions using conformal symmetry and two distinct approaches to N-C geometry.

M. Sharif and S. Nazir [45,46] investigated wormhole (WH) solutions through different approaches such as N-C geometry and the equation of state. Mustafa and colleagues [47] obtained WH solutions using conformal symmetry in the N-C geometry, within the framework of gravitational theory $F(T,T_G)$. Gaussian and Lorentzian matter distributions were utilized as N-C geometric sources in two different $F(T,T_G)$ gravity models. Shamir et al. [48] also applied Gaussian and Lorentzian N-C geometry in modified gravity theories, discovering stable spherically symmetric wormhole solutions in $f(R)$ gravity and proving the violation of the null energy condition (NEC). Banerjee and his colleagues introduced nonexotic matter and isotropic pressure in static spherical WH solutions in the context of $f(R,\mathcal{T})$ gravity [49]. Mustafa and his colleagues [50–60] conducted research on spherical WH solutions in different modified theories of gravity using different approaches. Alencar et al. [61] analyzed the Ellis–Bronnikov wormhole within asymptotically safe gravity on the Planck scale, demonstrating that compliance with radial energy conditions at the throat radius is guaranteed by asymptotic safety. It was determined that quantum gravitational effects support Einstein's field equations, requiring exotic matter for the formation of WH space–time [62–85].

In their research, Sharma and Ghosh [86] examined the energy needs of the embedded Ellis–Bronnikov wormhole (WH) and its extended form in a five-dimensional warped background. They discovered that the diminished warp factor meets the weak energy conditions and enhances other energy conditions when compared to the four-dimensional scenario. Hassan and his team studied the stability of WH solutions by analyzing two particular shape functions within the framework of $f(Q)$ gravity, with Q representing the non-metricity tensor. Shamir and colleagues investigated WH formations in $f(R,\varphi,X)$ gravity theory, with φ as the scalar potential and X as the kinetic term [87]. The researchers studied how a fluid with no trace behaves when subject to specific equations of state parameters and found that the chosen shape functions failed to meet the energy conditions. G. Mustafa and colleagues [88] discovered possible wormhole solutions that satisfy energy requirements within $f(Q)$ gravity by making use of a spacetime embedded subject to the Karmarkar condition. Shekh et al. [89] studied the physical constraints on accelerated emergent $f(Q)$ gravity model. Zwicky was the first to propose the presence of dark matter in galaxies by utilizing the virial theorem [90]. According to Rahaman et al. [91], galactic halos may have the ability to host traversable wormholes due to the NFW density profile and flat rotation curves found in galaxies [92–95].

In this study, we investigate generalized Ellis–Bronnikov and embedded wormhole solutions in $F(T,T_G)$ gravity with anisotropic matter sources. Using observational data from the $M87$ galaxy, we analyze energy conditions for wormhole formation under three distinct dark matter halo models. The results confirm that the violation of energy conditions, driven by exotic matter, is crucial for wormhole formation in this framework. Exploration of wormhole solutions in $F(T,T_G)$ gravity with anisotropic matter. Analysis of energy conditions using $M87$ galaxy data and three dark matter halo models. Violation of energy conditions confirms the role of exotic matter in wormhole formation.

The present study is organized in the following structure: We start with an introduction 1 about this subject, Section 2 concentrates on the assessment of $F(T,T_G)$ gravity and investigation of the wormhole (WH) geometry while also deriving the field equations within this section. Section 3 examines the energy conditions relevant to gravity involving the $F(T,T_G)$ theory. Section 4 presents two separate models along with their related field equations. Sections 5 and 6 discuss the shape functions and solutions embedded in wormholes. In Section 7, the dark matter halos for scalar field dark matter (SFDM), ultra-relativistic clusters (URC), and cold dark matter Navarro–Frenk–White (CDM-NFW) distributions are discussed. The last conclusion of our results 9.

2. $F(T, T_G)$ gravity

This section presents the new gravity model $F(T, T_G)$. Kofinas and his team suggested a new torsional constant T_G in the $F(T)$ formalism in order to obtain a teleparallel version of the Gauss–Bonnet (GB) term. Moreover, the symbol G will be used to symbolize the GB term.

$$\mathbf{h}\mathcal{G} = \mathbf{h}T_G + \mathfrak{D},$$

where total divergence is denoted with $\mathfrak{D}$ and $\mathcal{G}$ is known as the teleparallel invariant, which is defined as:

$$\mathcal{G} = \mathcal{R}^2 - 4\mathcal{R}_{\mu\nu}\mathcal{R}^{\mu\nu} + \mathcal{R}_{\mu\nu\alpha\beta}\mathcal{R}^{\mu\nu\alpha\beta}$$

and

$$T_G = \Big(\mathcal{K}^{a_2}_{b}\mathcal{K}^{a_1}_{ea}\mathcal{K}^{a_3}_{fc}\mathcal{K}^{a_4}_{d} + 2\mathcal{K}^{a_3}_{eb}\mathcal{K}^{a_1a_2}_{a}\mathcal{K}^{ea_4}_{c,d} - 2\mathcal{K}^{a_3}_{eb}\mathcal{K}^{a_1a_2}_{a}\mathcal{K}^{e}_{fc}\mathcal{K}^{fa_4}_{d} + 2\mathcal{K}^{a_3}_{eb}\mathcal{K}^{a_1a_2}_{a}\mathcal{K}^{ea_4}_{f}\mathcal{K}^{f}_{cd}\Big)\delta^{abcd}_{a_1a_2a_3a_4},$$

The Kronecker delta's determinant is denoted by δ. The tensor-like torsion in the expression $T_{\mathcal{G}}$ is raised to the power of four. The primary tensors of importance, like contusion and torsion, can be expressed as:

$$\mathcal{K}_{abc} = -\mathcal{K}_{bac} = -\frac{1}{2}(T_{bca} - T_{cab} + T_{abc}),$$

and

$$T^a_{bc} = \mathbf{h}^a_\alpha(\partial_b\mathbf{h}^\alpha_c - \partial_c\mathbf{h}^\alpha_b) = \Gamma^a_{cb} - \Gamma^a_{bc}.$$

The modified gravity action $F(T, T_G)$ can be expressed as:

$$S = \frac{1}{2\kappa^2}\int \mathbf{h}[F(T, T_G) + \mathcal{L}_{\mathrm{m}}]d^4x.$$

The Lagrangian in this situation is represented by: $\mathcal{L}_{\mathrm{m}}$, where $\kappa^2 = 1$, and $\mathbf{h} = \det(\mathbf{h}^a_\beta) = \sqrt{-\mathrm{g}}$, where g is the determinant of the metric tensor. The modified gravity framework, which involves varying $\mathbf{h}^a_\beta$ action, leads to the derivation of modified field equations.

$$\begin{aligned}
&-(F(T, T_G)) - TF_T(T, T_G) - T_{\mathcal{G}}F_{T_G}(T, T_G)\eta^{ij}\\
&= 2(H^{[ik]j} - H^{[kj]i} + H^{[ji]k})_{,k} + 2(H^{[ji]k} + H^{[ik]j} - H^{[kj]i})C^d_{dk}\\
&\quad +(2H^{[ik]d} + H^{dki})C^j_{kd} + 4H^{[dj]k}C^i_{dk} + T^i_{kd}H^{kdj} - \mathbf{h}^{ij},
\end{aligned} \tag{1}$$

where

$$\begin{aligned}
H^{ijk} &= F_T(T, T_G)(\eta^{ik}\mathcal{K}^{jd}_{d} - \mathcal{K}^{jki}) + F_{T_{\mathcal{G}}}(T, T_G)\\
&\quad \Big(\epsilon^{kprt}(e\epsilon^{i}_{dlf}\mathcal{K}^{jk}_{p}\mathcal{K}^{d}_{qr} + \epsilon_{qdlf}\mathcal{K}^{il}_{p}\mathcal{K}^{jd}_{r}\\
&+ \epsilon^{ij}_{lf}\mathcal{K}^{l}_{dp}\mathcal{K}^{d}_{qr})\mathcal{K}^{q,f}_{t} + \epsilon^{kprt}\epsilon^{ij}_{ld}\mathcal{K}^{fd}_{p} \times (\mathcal{K}^{l}_{fr,t} - \frac{1}{2}\mathcal{K}^{l}_{fq}C^{q}_{tr}) + \epsilon^{kprt}\epsilon^{il}_{df}\mathcal{K}^{df}_{p}\\
&\times (\mathcal{K}^{j}_{kr,t} - \frac{1}{2}\mathcal{K}^{j}_{lq}C^{q}_{tr})\Big) + \epsilon^{kprt}\epsilon^{i}_{ldf}\\
&\quad \Big((F_{T_{\mathcal{G}}}(T, T_G)\mathcal{K}^{jl}_{p}\mathcal{K}^{df}_{r})_{,t} + F_{T_{\mathcal{G}}}(T, T_G)C^{q}_{pt}\mathcal{K}^{jl}_{q}\mathcal{K}^{df}_{r}\Big),
\end{aligned} \tag{2}$$

and

$$\mathbf{h}^{ij} = F_T(T, T_G)\epsilon^{i}_{lke}\epsilon^{jabe}\mathcal{K}^{l}_{fa}\mathcal{K}^{fk}_{b},$$

$$F_T(T, T_G) = \frac{dF(T, T_G)}{dt}, \qquad F_{T_{\mathcal{G}}}(T, T_G) = \frac{dF(T, T_G)}{dT_G}.$$

The symmetric metric defines the geometry of the WH [45] as.

$$ds^2 = e^{\lambda(r)}dt^2 - e^{\nu(r)}dr^2 - r^2d\Omega^2. \tag{3}$$

where $d\Omega^2 = d\theta^2 + sin^2\theta d\phi^2$.

- The redshift function is defined as $\lambda(r)$ equal to twice the gravitational potential function $\Phi(r)$. It is observed that the essential redshift function does not have to comply with any horizon constraints, thus enabling a round-trip journey. Because of this intellectual aspect, $\lambda(r)$ must remain finite every where.
- Moreover, $e^{\nu(r)} = (1-W(r)/r)^{-1}$, with $W(r)$ being a radial function of the coordinate r, is referred to as the shape function due to its role in determining the WH geometry.
- The presence of WH solution $W(r_0) = r_0$ and the flaring out condition is defined as $(W - W'r)/W^2 > 0$. Additionally, the conditions $W'(W_0) < 1$ and $1 - W(r)/r > 0$ are further requirements for WHs solutions.
- These all kinds of conditions lead us to violate the energy conditions.

For considering the WH's material composition, we use the stress–energy tensor with anisotropic fluid. Its given with this equation [47]:

$$\mathcal{T}_{\mu\nu} = (\rho + p_t)\upsilon_\lambda\upsilon_\nu - p_t\mathrm{g}_{\lambda\nu} + (p_r - p_t)\xi_\lambda\xi_\nu,$$

where the components of the 4-velocity vector (υ_λ) are: $\upsilon^\lambda = e^{-\lambda}\delta^\lambda_0$ and $\xi^\lambda = e^{-\nu}\delta^\lambda_1$ which follows $\upsilon^\lambda\upsilon_\lambda = -\xi^\lambda\xi_\lambda = 1$. The stress–energy tensor consists of tangential pressure, energy density with radial pressure, with the condition that the tangential pressure is perpendicular to ξ_λ and the radial pressure is parallel to ξ_λ. The diagonal tetrad is given as:

$$\mathbf{h}^a_\nu = diag\left(e^{-\lambda(r)}, \left(1 - \frac{W(r)}{r}\right)^{-\frac{1}{2}}, r, rsin\theta\right). \tag{4}$$

The torsion scalar is:

$$T = \frac{2}{r^2}\left(1 - \frac{W(r)}{r}\right)\frac{4\lambda'(r)}{r}\left(1 - \frac{W(r)}{r}\right) \tag{5}$$

and we get

$$\begin{aligned}
T_G &= \frac{12\lambda'(r)W(r)W'(r)}{r^4} - \frac{8(\lambda'(r))^2W(r)}{r^3} \times \left(1 - \frac{W(r)}{r}\right)\\
&\quad - \frac{8\lambda''(r)W(r)}{r^3} \times \left(1 - \frac{W(r)}{r}\right)\\
&\quad - \frac{8\lambda'(r)W'(r)}{r^3} - \frac{12\lambda'(r)W^2(r)}{r^5} + \frac{8\lambda'(r)W(r)}{r^4},
\end{aligned} \tag{6}$$

It is noted that $\lambda(r)$ cannot be considered as constant. otherwise T_G vanishes. Using Eqs. (3) and (6) in Eq. (1), field equations become

$$\begin{aligned}
\rho &= \frac{2W'(r)}{r^2}F_T(T, T_G) + F(T, T_G) - TF_T(T, T_G) - T_GF_{T_{\mathcal{G}}}(T, T_G)\\
&\quad - \frac{4}{r}\left(1 - \frac{W(r)}{r}\right)F_{TT}(T, T_G)T'\\
&\quad + \frac{4}{r^3}\left(\frac{5W(r)}{r} - 2 - \frac{3W^2(r)}{r^2} - 3W'(r)\left(1 - \frac{W(r)}{r}\right)\right)\\
&\quad F_{T_GT_G}(T, T_G)T'_G + \frac{8}{r^2}\left(1 - \frac{W(r)}{r}\left(2 - \frac{W(r)}{r}\right)\right)\\
&\quad \times (F_{T_GT_GT_G}(T, T_G)(T'_G)^2 + F_{T_GT_G}(T, T_G)T''_G),
\end{aligned} \tag{7}$$

$$\begin{aligned}
p_r &= -F(T, T_G) + \left(\frac{2}{r^2}\left(1 - \frac{2W(r)}{r}\right) - \frac{4\lambda(r)}{r^2}\left(1 - \frac{W(r)}{r}\right)\right)\\
&\quad \times F_T(T, T_G) + T_GF_{T_G}(T, T_G)\\
&\quad + \frac{24\lambda(r)}{r^3}\left(1 - \frac{W(r)}{r}\right)^2F_{T_GT_G}(T, T_G)(T'_G)^2,
\end{aligned} \tag{8}$$

$$\begin{aligned}
p_t &= -F(T, T_G) + \left(\frac{1}{r}\left(2 - \frac{W(r)}{r} - \frac{W'(r)}{r}\right)\left(\frac{1}{r} - \frac{\lambda(r)}{r}\right)\right.\\
&\quad \left. + 2\left(1 - \frac{W(r)}{r}\right)\left(\frac{2\lambda(r)}{r^2} + \frac{\lambda^2(r)}{r^2}\right)\right)\\
&\quad \times F_T(T, T_G) + T_GF_{T_G}(T, T_G) + 2\left(1 - \frac{W(r)}{r}\right)\left(\frac{1}{r} - \frac{\lambda(r)}{r}\right)F_{TT}(T, T_G)T'\\
&\quad + \left(-\frac{12\lambda}{r^3}\left(W'(r) - \frac{W(r)}{r^2}\right) \times \left(1 - \frac{W(r)}{r}\right)\right.\\
&\quad \left. - \frac{8}{r}\left(\frac{2\lambda(r)}{r^2} + \frac{\lambda^2(r)}{r^2}\right)\left(1 - \frac{W(r)}{r}\right)^2\right)F_{T_GT_G}(T, T_G)T'_G\\
&\quad + \frac{8\lambda(r)}{r^2}\left(1 - \frac{W(r)}{r}\right)^2 \times (F_{T_GT_GT_G}(T, T_G)(T'_G)^2 + F_{T_GT_G,}(T, T_G)T''_G),
\end{aligned} \tag{9}$$

3. Energy conditions

Five conditions related to energy conditions are recognized: null energy condition (NEC), weak energy condition (WEC), dominant energy condition (DEC), strong energy condition (SEC), and trace energy condition (TEC). In the context of the modified gravity being examined, the energy conditions can be defined as follows [46]:

$$\mathcal{T}_{\mu\nu}^{(eff)} = \mathcal{T}_{\mu\nu}^{(m)} + \mathcal{T}_{\mu\nu}^{(\mathcal{H})},$$

where $\mathcal{T}_{\mu\nu}^{(\mathcal{H})}$ denotes the terms related to the dark source. Below, we present the mathematical expression of the energy conditions:

- NEC: $\forall i, \quad \rho + p_i \geq 0.$
- WEC: $\rho \geq 0 \quad \text{and} \quad \forall i, \ \rho + p_i \geq 0.$
- DEC: $\rho \geq 0 \quad \forall i, \quad \rho \pm p_i \geq 0.$
- SEC: $\rho + p_i \geq 0 \quad \text{and} \quad \forall i, \quad \rho + \sum p_i \geq 0.$
- TEC: $\rho - p_i \geq 0 \quad \text{and} \quad \forall i, \quad \rho - \sum p_i \geq 0.$

4. First model of $F(T, T_G)$ gravity

Herein, we shall consider a specific model for $F(T, T_G)$ gravity [45–47], which yields:

$$F(T, T_G) = \Psi_1 \left(-\frac{\Psi_3 T_G}{\sqrt{T}} \right)^{\Psi_2}, \tag{10}$$

where Ψ_1, Ψ_3, and Ψ_2 are the model parameters. It is essential to mention that the parameter Ψ_2 will remain equal to one throughout the analysis to achieve physically viable results. For the other parameters, only positive values between zero and one should work for the current analysis. The negative value of energy density for $F(T, T_G)$ should be negative, which is unsuitable for WH solutions. By using Eq. (10) in Eqs. (7)–(9), we obtain the respective modified form of the field equations:

$$\rho = 2^{\frac{\Psi_2}{2}-3} \Psi_1 \chi_2^{\Psi_2} \left[-\frac{\Psi_2 r^3 b'(r)}{(r-b(r))^2 \lambda'(r)} + \frac{1024 \left(\Psi_2 - 1\right) \Psi_2 \chi_{18} (r-b(r))^2}{r \chi_{19}^3} \right.$$
$$\left. -4 \Psi_2 - \chi_3 + \chi_{20} + 8 \right], \tag{11}$$

$$p_r = 2^{\frac{\Psi_2}{2}-3} \Psi_1 \chi_2^{\Psi_2} \left[\chi_{21} - \frac{48 \left(\Psi_2 - 1\right) \Psi_2 \chi_8 (r-b(r))^2 \lambda(r)}{r \chi_9^2} \right], \tag{12}$$

$$p_t = 2^{\frac{\Psi_2}{2}-4} \Psi_1 \chi_2^{\Psi_2} \left[\frac{2048 \left(\Psi_2 - 1\right) \Psi_2 r \chi_{18} \left(\frac{b(r)}{r} - 1\right)^2 \lambda(r)}{\chi_{19}^3} \right.$$
$$\left. +16 \Psi_2 - \chi_3 - \chi_{22} + \chi_{23} - 16 \right], \tag{13}$$

where χ_i, $i = 1, \ldots, 23$ are given in the Appendix A.

5. Second model of $F(T, T_G)$ gravity

Here, we shall take another specific model for $F(T, T_G)$ gravity [45–47], which is expressed as:

$$F(T, T_G) = \Psi_1 \left(\Psi_2 T_G + T^2 \right) + \Psi_3 \left(\Psi_4 T_G + T^2 \right)^2 - T. \tag{14}$$

where Ψ_1, Ψ_2, Ψ_3, and Ψ_4 are the model parameters. It is also essential to mention that the parameter Ψ_2 will remain equal to one throughout the analysis to achieve the physically viable results for the second model of $F(T, T_G)$ gravity. For the other involved parameters, only positive but small values, i.e., $(0, 1)$ for Ψ_3 and Ψ_4, should be feasible for the physically viable WH solutions in this analysis model. The negative value of energy density for $F(T, T_G)$ should be negative, which is unsuitable for wormhole solutions. Additionally, the positive values of parameter Ψ_1 are suitable to find viable regions for the WH solution.

- Utilizing Eq. (14) in Eqs. (7)–(9) yields a set of equations for the initial model of $F(T, T_G)$ gravity (see Box I).

We adopt the restriction that $\lambda(r) = 2\Phi(r)$ must be finite everywhere within the WH space–time since an event horizon cannot be achieved in WH space–time. In the present part, we take the redshift function as [45–47].

$$\Phi = -\frac{\varrho}{r}, \tag{18}$$

where ϱ is constant.

6. Embedded WH solutions

This research investigates embedded wormhole (WH) models through two distinct approaches. The first approach examines a broader category of embedded WH solutions by exploring the Karmarkar condition [96] within class-1, as well as the Ellis and embedded Bronnikov spacetimes. The Karmarkar condition's fundamental framework is based on class-1 embedded solutions in Riemannian space. Eisenhart studied the appropriate configuration for these class-1 embedded solutions [97], which is derived from the properties of the Gauss equation.

$$\mathcal{R}_{mnpq} = 2\epsilon \, b_{m\,[p} b_{q]n}. \tag{19}$$

The equation referred to as the Codazzi equation is expressed as:

$$b_{m[n;p]} = \Gamma^q_{[n\,p]} \, b_{mq} - \Gamma^q_{m\,[n} \, b_{p]q}. \tag{20}$$

In the provided formula, square brackets denote anti-symmetrization, where ϵ takes values of ± 1, and b_{mn} represents the coefficients of the second differential form. By utilizing Eqs. (19) and (20), we can derive the Karmarkar condition as demonstrated below:

$$R_{2323} R_{1414} = R_{1224} R_{1334} + R_{1212} R_{3434}, \tag{21}$$

where $R_{2323} \neq R_{1414} \neq 0$. We can use the suitable Riemannian tensor in Eq. (21), we have:

$$\frac{\lambda'(r)\nu'(r)}{1 - e^{\nu(r)}} - \left\{ \lambda'(r)\nu'(r) + \lambda'(r)^2 - 2\left[\lambda''(r) + \lambda'(r)^2 \right] \right\} = 0, \qquad e^{\nu(r)} \neq 1, \tag{22}$$

By solving (22), we have

$$e^{\nu(r)} = 1 + \Psi e^{\lambda(r)} \lambda'^2(r), \tag{23}$$

In this case, Ψ symbolizes a constant involved in integration. By following the steps detailed in [88], we derive the embedded shape function.

$$W(r) = r - \frac{r^5}{r^4 + W_0^4 (W_0 - \omega)} + \omega, \quad 0 < \omega < W_0, \tag{24}$$

In this situation, W_0 represents the diameter of the wormhole's entrance. We will continue by studying the generalized Ellis–Bronnikov spacetime [86], which is an ultra-static wormhole model. This is the second wormhole solution derived by embedding, explained as follows:

$$ds^2 = -dt^2 + dl^2 + r^2(l) \left[d\theta^2 + \sin^2(\theta) d\phi^2 \right], \tag{25}$$

with

$$r(l) = \left[W_0^m + l^m \right]^{1/m}. \tag{26}$$

The formulas presented above use l to denote the proper radial distance, which is also referred to as the tortoise coordinate and is applicable to both embedded solutions. As previously stated, X_0 indicates the diameter of the WH's throat, with m denoting the WH parameter, under the constraint ($m \geq 2$). We can write Eq. (3) as:

$$ds^2 = -dt^2 + \frac{dr^2}{\left[1 - \frac{W(r)}{r} \right]} + d\Omega^2. \tag{27}$$

$$\rho = \left[-\frac{2\left(144\beta_3\Psi_4^2 r^{12}(r-b(r))b'(r)^3\lambda'(r)+\zeta_4 r^3 b'(r)+8\left(\Psi_3\zeta_{14}+4\Psi_1\zeta_5 r^{10}(r-b(r))^2\right)-8\zeta_1\right)}{r^{20}}\right], \tag{15}$$

$$p_r = \left[\frac{\zeta_{30}r^{17}(4b(r)(\lambda(r)-1)-4r\lambda(r)+2r)+8r^{15}(r-b(r))^2\lambda'(r)-\Psi_3\Psi_4^2\zeta_{21}r^9(r-b(r))^2\lambda(r)+\zeta_{22}}{r^{20}}\right], \tag{16}$$

$$p_t = \left[\frac{8r^{15}(r-b(r))^2\lambda'(r)-64\Psi_3\Psi_4^2\zeta_{25}r^9(r-b(r))^2\lambda(r)+\zeta_{27}+\zeta_{30}-4\zeta_{18}r^5\left(8\Psi_3\Psi_4\zeta_{19}+\Psi_1\Psi_2 r^{10}\right)}{r^{20}}\right], \tag{17}$$

where ζ_j, $j = 1,\ldots,30$ are given in the Appendix B.

Box I.

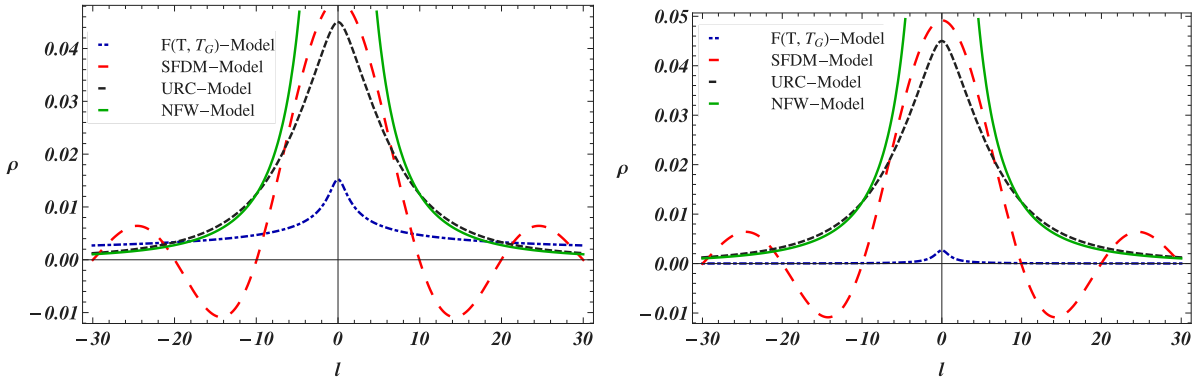

Fig. 1. Illustrates how ρ varies with $\Psi_1 = 0.02$, $\Psi_3 = 0.11$, $\Psi_2 = 1$, $\varrho = -0.01$, $\omega = 0.06$ $m = 2$, and $W_0 = 0.09$ in scenarios such as $F(T, T_G)$ gravity, URC profile, CDM halo with NFW profile, and SFDM profile.

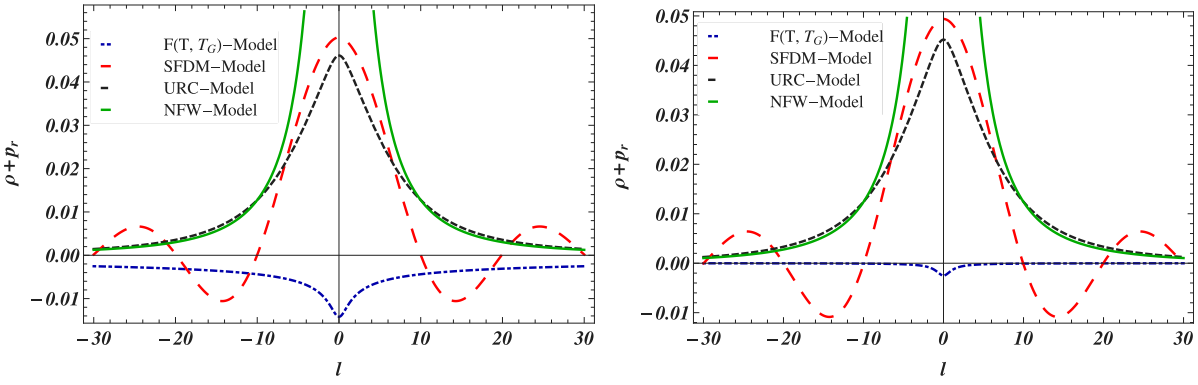

Fig. 2. Illustrates the pattern of $\rho + p_r$ with specific values of $\Psi_1 = 0.02$, $\Psi_3 = 0.11$, $\Psi_2 = 1$, $\varrho = -0.01$, $\omega = 0.06$ $m = 2$, and $W_0 = 0.09$ across four scenarios including $F(T, T_G)$ gravity, URC profile, CDM halo with NFW profile, and SFDM profile.

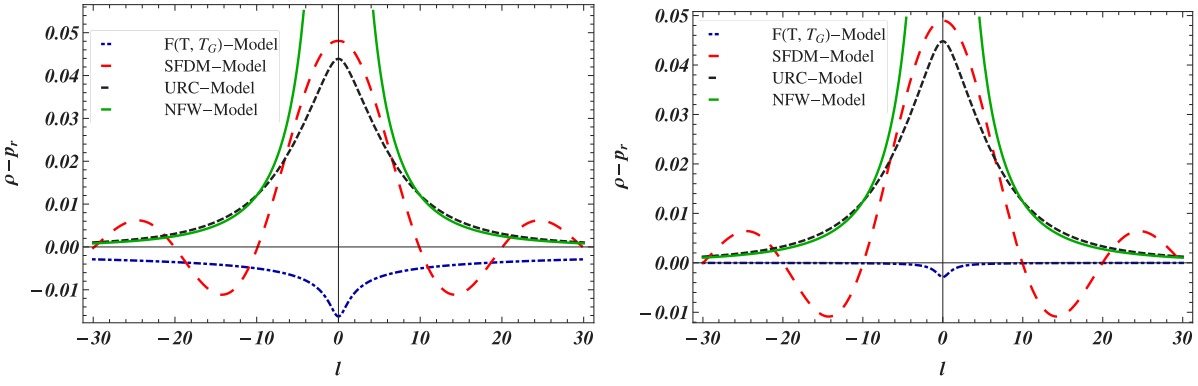

Fig. 3. Illustrates how $\rho - p_r$ changes when $\Psi_1 = 0.02$, $\Psi_3 = 0.11$, $\Psi_2 = 1$, $\varrho = -0.01$, $\omega = 0.06$ $m = 2$, and $W_0 = 0.09$ in four distinct scenarios: $F(T, T_G)$ gravity, URC profile, CDM halo with NFW profile, and SFDM profile.

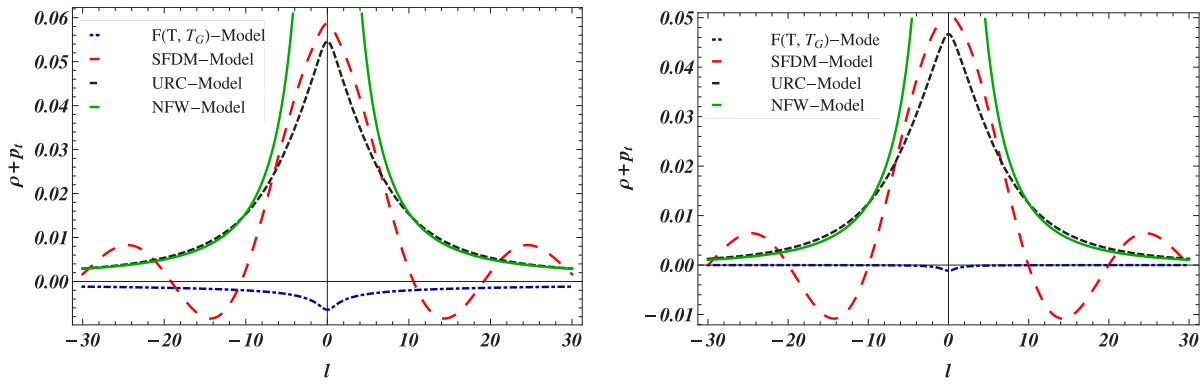

Fig. 4. The relationship between $\rho + p_t$ and the specified parameters: $\Psi_1 = 0.02$, $\Psi_3 = 0.11$, $\Psi_2 = 1$, $\varrho = -0.01$, $\omega = 0.06$, $m = 2$, and $W_0 = 0.09$, in scenarios such as $F(T, T_G)$ gravity, URC profile, CDM halo with NFW profile, and SFDM profile.

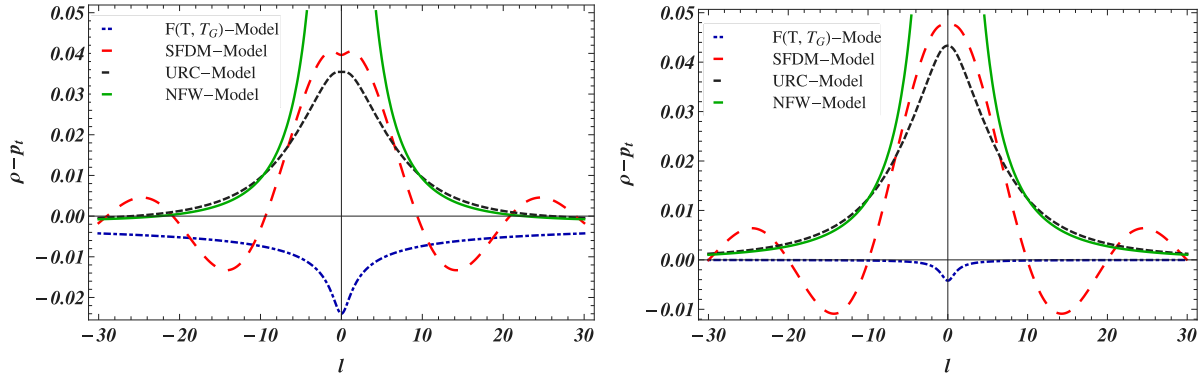

Fig. 5. This illustrates the behavior of $\rho - p_t$ with $\Psi_1 = 0.02$, $\Psi_3 = 0.11$, $\Psi_2 = 1$, $\varrho = -0.01$, $\omega = 0.06$, $m = 2$, and $W_0 = 0.09$ for four cases: $F(T, T_G)$ gravity, URC profile, CDM halo with NFW profile, and SFDM profile.

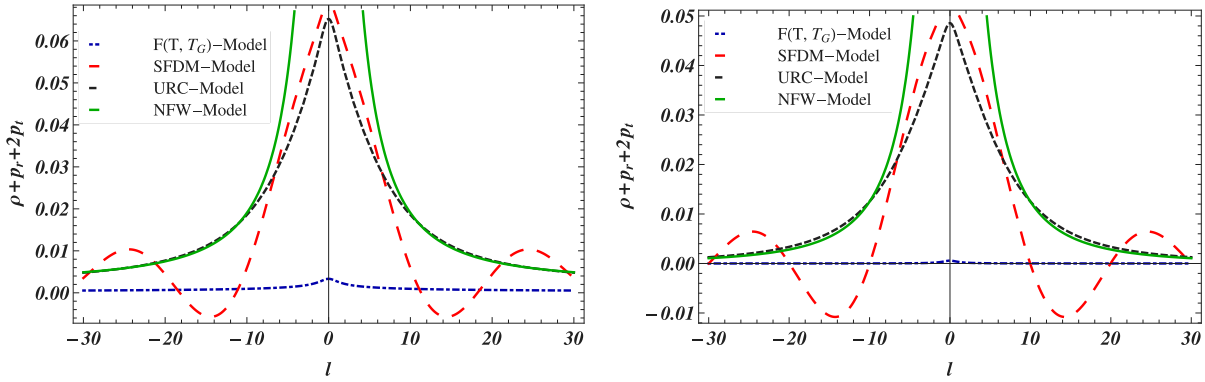

Fig. 6. The behavior of $\rho + p_r + 2p_2$ is shown with parameters $\Psi_1 = 0.02$, $\Psi_3 = 0.11$, $\Psi_2 = 1$, $\varrho = -0.01$, $\omega = 0.06$, $m = 2$, and $W_0 = 0.09$ for four cases: $F(T, T_G)$ gravity, URC profile, CDM halo (NFW profile), and SFDM profile.

The radial coordinate r and the radial distance l are connected through the following embedding equation.

$$dl^2 = \frac{dr^2}{\left[1 - \frac{W(r)}{r}\right]} \tag{28}$$

Finally, we have obtained this function:

$$W(r) = r - r^{(3-2m)}\left(r^m - W_0^m\right)^{(2-\frac{2}{m})}. \tag{29}$$

For $m = 2$, the geometry corresponds to the Ellis–Bronnikov wormhole, which features a spacetime without horizons. We employ two distinct embedded wormhole solutions from Eqs. (12) and (17), linking the radial coordinate r and the radial distance l through Eq. (14) (see Fig. 13).

7. Dark matter profiles

Dark matter is a puzzling component of the universe, accounting for 29.6% of its mass energy, followed by dark energy at 67.4% and atomic matter at 4%. Dark matter is essential in the formation and evolution of galaxies. The widespread presence of traversable wormholes could potentially be achieved within it, thanks to energy condition violations. This research will investigate how different types of DM profiles impact enclosed wormhole solutions linked to various DM halos.

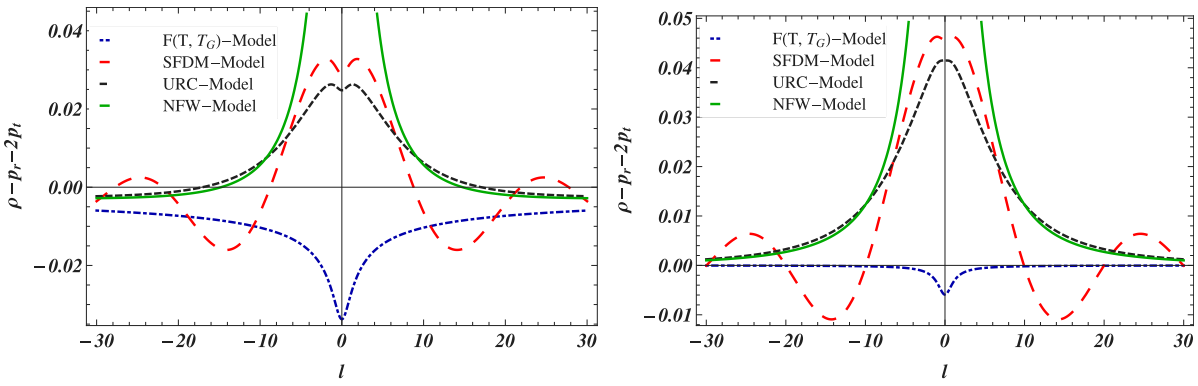

Fig. 7. Illustrates the behavior of $\rho - p_r - 2p_t$ with parameters $\Psi_1 = 0.02$, $\Psi_3 = 0.11$, $\Psi_2 = 1$, $\varrho = -0.01$, $\omega = 0.06$, $m = 2$, and $W_0 = 0.09$ for four scenarios: $F(T, T_G)$ gravity, URC profile, CDM halo with NFW profile, and SFDM profile.

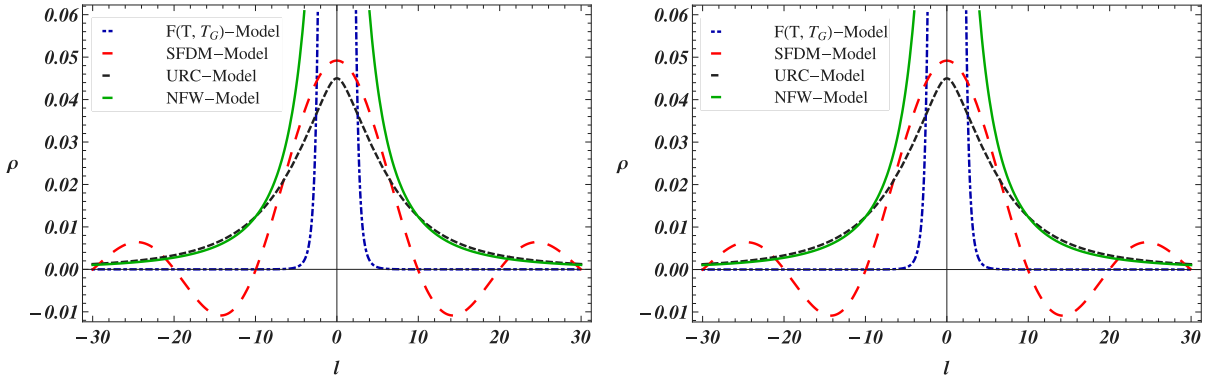

Fig. 8. This illustrates the behavior of ρ with the parameters $\Psi_1 = -7.2$, $\Psi_3 = 0.11$, $\Psi_2 = 1$, $\Psi_4 = 0.05$, $\varrho = -0.01$, $\omega = 0.06$, $m = 2$, and $W_0 = 0.09$ for four distinct scenarios: $F(T, T_G)$ gravity, the URC profile, the CDM halo with the NFW profile, and the SFDM profile.

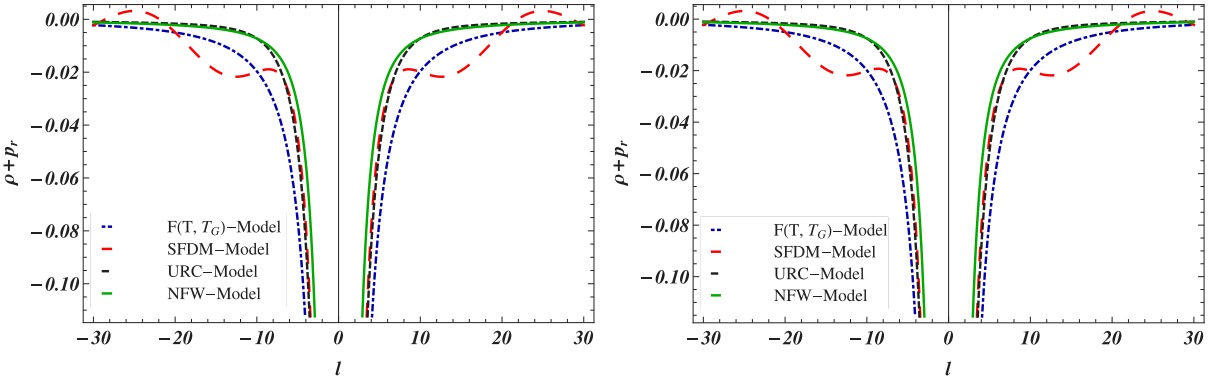

Fig. 9. This illustrates the behavior of $\rho + p_r$ with parameters $\Psi_1 = -7.2$, $\Psi_3 = 0.11$, $\Psi_2 = 1$, $\Psi_4 = 0.05$, $\varrho = -0.01$, $\omega = 0.06$, $m = 2$, and $W_0 = 0.09$ for four different cases: $F(T, T_G)$ gravity, the URC profile, the CDM halo with the NFW profile, and the SFDM profile.

a. URC profile: The authors in [98] show that the (URC) is a successful approach for illustrating mass distribution in disk systems. The URC profile of the DM halo, as defined by [98], is also characterized by:

$$\rho(r) = \frac{\rho_s r_s^3}{(r + r_s)(r^2 + r_s^2)}, \tag{30}$$

In Eq. (30), r_s is the radius parameter, and ρ_s is the central density of the dark matter halo according to the Universal Rotation Curve (URC). In this research, we utilize the parameters $\rho_s = 6.9 \times 10^6 \mathrm{M}_\odot/\mathrm{kpc}^3$ and $r_s = 91.2$ kpc, obtained from observations of the M87 galaxy [99].

b. The CDM halo with NFW profile: The Navarro–Frenk–White (NFW) profile is the most popular model for explaining the density profile of cold dark matter (CDM) distribution [100]. Based on N-body simulations [100,101], the NFW profile is written in the following way:

$$\rho(r) = \frac{\rho_s}{(r/r_s)(1 + r/r_s)^2}, \tag{31}$$

In this case, r_s indicates the radius parameter, and ρ_s stands for the central density of the universe. The central density of the M87 galaxy is $\rho_s = 0.008 \times 10^{7.5}$ $\mathrm{M}_\odot/\mathrm{kpc}^3$ [44], with a size of $r_s = 130$ kpc as stated in Ref. [18].

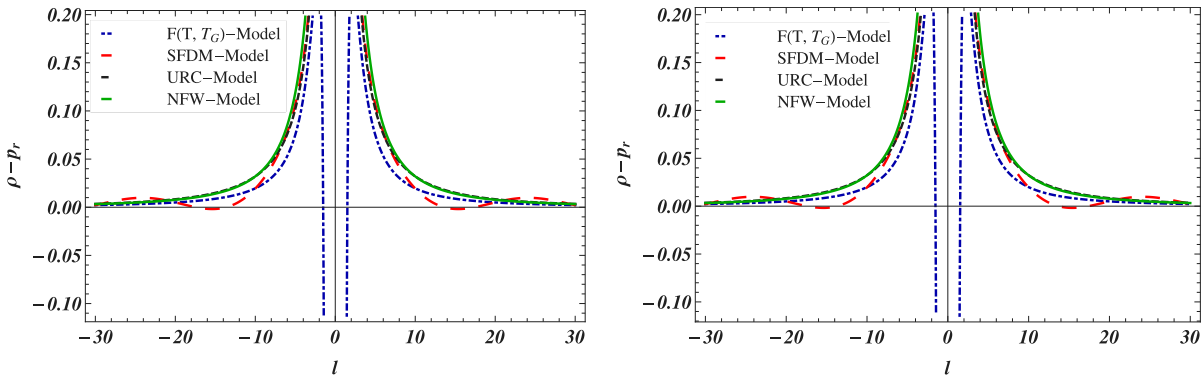

Fig. 10. This illustrates the behavior of $\rho - p_r$ under the conditions $\Psi_1 = -7.2$, $\Psi_3 = 0.11$, $\Psi_2 = 1$, $\Psi_4 = 0.05$, $\varrho = -0.01$, $\omega = 0.06$, $m = 2$, and $W_0 = 0.09$ across four different scenarios: $F(T, T_G)$ gravity, URC profile, CDM halo with NFW profile, and SFDM profile.

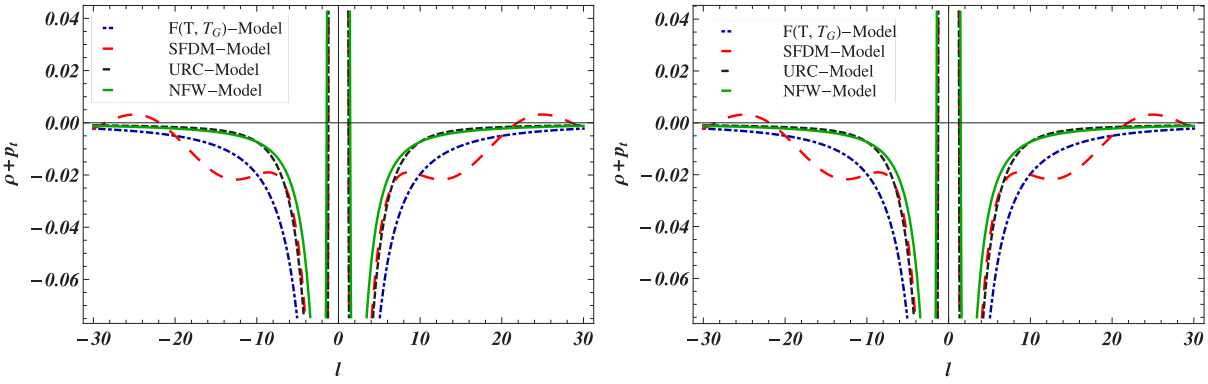

Fig. 11. This illustrates the behavior of $\rho + p_t$ with the parameters $\Psi_1 = -7.2$, $\Psi_3 = 0.11$, $\Psi_2 = 1$, $\Psi_4 = 0.05$, $\varrho = -0.01$, $\omega = 0.06$, $m = 2$, and $W_0 = 0.09$ across four different scenarios: $F(T, T_G)$ gravity, the URC profile, the CDM halo with the NFW profile, and the SFDM profile.

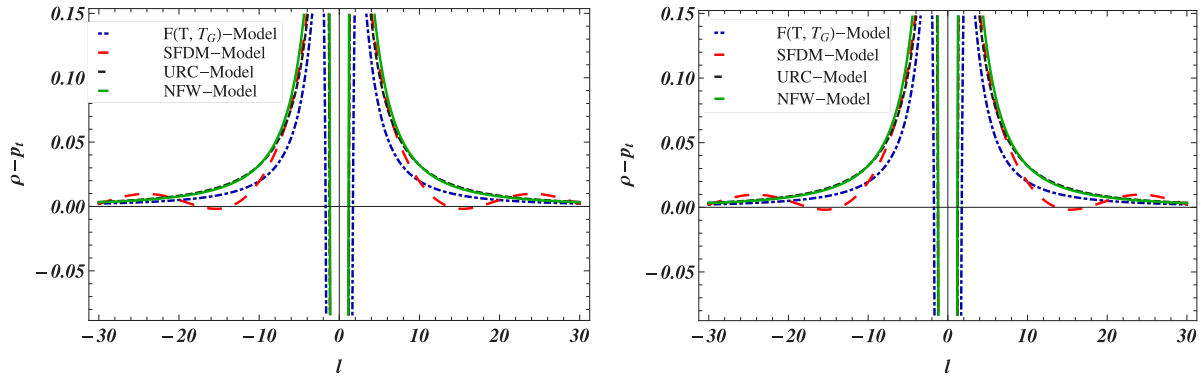

Fig. 12. This illustrates the behavior of $\rho - p_t$ given the parameters $\Psi_1 = -7.2$, $\Psi_2 = 1$, $\Psi_3 = 0.11$, $\Psi_4 = 0.05$, $\varrho = -0.01$, $\omega = 0.06$, $m = 2$, and $W_0 = 0.09$ across four different scenarios: $F(T, T_G)$ gravity, URC profile, CDM halo with an NFW profile, and SFDM profile.

c. The SFDM profile: The SFDM model [102,103] for the dark matter halo is expressed as follows.

$$\rho(r) = \frac{\rho_s \sin(\pi r/r_s)}{\pi r/r_s}. \tag{32}$$

- In Eq. (32), r_s signifies the characteristic radius, whereas ρ_s indicates the central density of the SFDM (scalar field dark matter) halo. The Milky Way galaxy has values of $\rho_s = 3.43\times10^7\,\mathrm{M_\odot/kpc^3}$ and $r_s = 15.7\,\mathrm{kpc}$ according to reference 49. In this research, we will assess the effectiveness of the achieved outcomes. Our main research interest lies in examining the energy constraints in the context of $F(T, T_G)$ gravity, particularly for two enclosed wormhole (WH) solutions. Furthermore, we will investigate the impact of dark matter halos on the URC, NFW, and SFDM profiles through an analysis of energy conditions.
- We utilize the embedded WH solutions obtained from Eqs. (24) and (29), which connect the radial location r and radial distance l using Eq. (26). Moreover, we include the URC, NFW, and SFDM profiles as energy density functions, substituting the existing gravitational energy density to evaluate their impact and efficacy on the energy conditions. Figs. 1 and 8 show the energy density profiles for $F(T, T_G)$ gravity models compared to the URC, NFW,

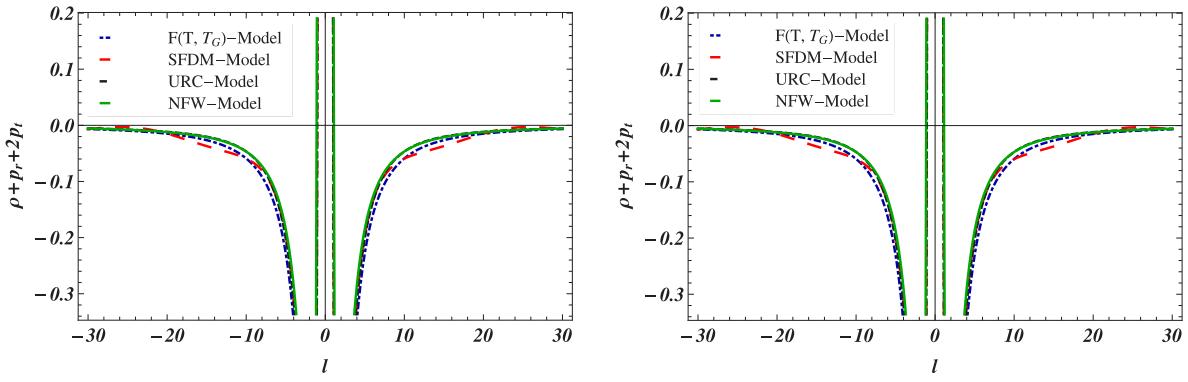

Fig. 13. The behavior of $\rho + p_r + 2p_t$ with the parameters $\Psi_1 = -7.2$, $\Psi_2 = 1$, $\Psi_3 = 0.11$, $\Psi_4 = 0.05$, $\varrho = -0.01$, $\omega = 0.06$, $m = 2$, and $W_0 = 0.09$ across four different scenarios: $F(T, T_G)$ gravity, the URC profile, the CDM halo using the NFW profile, and the SFDM profile.

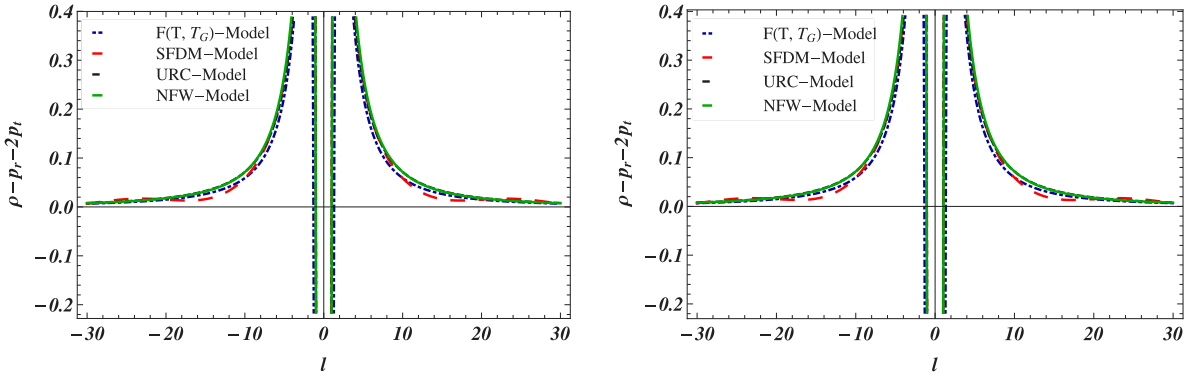

Fig. 14. The behavior of $\rho - p_r - 2p_t$ is analyzed for the following parameters: $\Psi_1 = -7.2$, $\Psi_2 = 1$, $\Psi_3 = 0.11$, $\Psi_4 = 0.05$, $\varrho = -0.01$, $\omega = 0.06$, $m = 2$, and $W_0 = 0.09$. This analysis is conducted across four different scenarios: $F(T, T_G)$ gravity, URC profile, CDM halo with an NFW profile, and SFDM profile.

and SFDM profiles. The energy density mostly stays positive, aside from the SFDM profile, which has positive values at its highest point but negative values at small distances. l.

- Figs. 2 and 9 Demonstrate the null energy condition (NEC), described as $\rho + p_r$, for the included wormhole solutions in both versions of $F(T, T_G)$ gravity. In the second scenario, there is a notable breach of the NEC, while in the first scenario, this breach is limited to specific instances of $F(T, T_G)$ gravity and SFDM. The presence of exotic matter in dark matter halos characterized by URC, NFW, and SFDM profiles is revealed through the violation of the NEC. These dark matter halos play a crucial role in the presence of embedded wormhole solutions.
- Figs. 3 and 10 display the contrast in characteristics of $\rho - p_r$ and $\rho + p_r$. The weak energy condition (WEC) violations in specific parts of the setups are depicted in Figs. 4 and 5 and 11 and 12 for both $F(T, T_G)$ gravity models. The SEC is represented as $\rho + p_r + 2p_2$ in Figs. 6 and 12 for both forms of $F(T, T_G)$ gravity and is observed to be negative in specific parts of the wormhole configurations. Ultimately, the breach of the trace energy condition (TEC) can be seen within certain radial distances. l as shown in Figs. 7 and 14 for both $F(T, T_G)$ gravity models.

8. Thin-shell around wormholes stability through radial linear perturbation

This section is devoted to presenting the behavior of shell radius around WH geometry. For this purpose, we use Schwarzschild BH as an outer manifold and inner geometry is traversable WH with two different choices of shape functions for details see the Refs. [104–111]. Then, we explore the effects choices of two shape functions. By using the Israel formalism, we develop the energy contents of matter located at the shell $r = \gamma$. It can be evaluated as:

$$\sigma_0 = -\frac{1}{4\pi\gamma_0}\left\{\sqrt{-\frac{2m}{\gamma_0}+1}-\sqrt{-\frac{b(\gamma_0)}{\gamma_0}+1}\right\},$$
$$p_0 = \frac{1}{8\pi\gamma_0^2}\left\{\frac{\gamma_0\left(b'(\gamma_0)-2\right)+b(\gamma_0)}{\sqrt{1-\frac{b(\gamma_0)}{\gamma_0}}}+\frac{2(\gamma_0-m)}{\sqrt{1-\frac{2m}{\gamma_0}}}\right\}, \tag{33}$$

where density and pressure at the equilibrium position are denoted with σ_0 and p_0, respectively. Now, we want to use linearized radial perturbation at $\gamma = \gamma_0$ to investigate the stable configuration of a developed thin-shell around WH geometry. We get the effective potential from the equation of motion of the shell as:

$$V(\gamma) = \frac{mb(\gamma)}{16\pi^2\gamma^4\sigma^2} - \frac{b(\gamma)^2}{64\pi^2\gamma^4\sigma^2} - \frac{b(\gamma)}{2\gamma} - \frac{m^2}{16\pi^2\gamma^4\sigma^2} - 4\pi^2\gamma^2\sigma^2 - \frac{m}{\gamma} + 1. \tag{34}$$

The energy conservation constraints are followed by stress–energy tensor components.

$$p\frac{d}{d\tau}(4\pi\gamma^2) + \frac{d}{d\tau}(4\pi\gamma^2\sigma) = 0, \tag{35}$$

which turns out to be

$$\sigma' = -\frac{2(\sigma + p(\sigma))}{\gamma}. \tag{36}$$

We can expand the effective potential as:

$$V(\gamma) = V(\gamma_0) + (\gamma - \gamma_0)V'(\gamma_0) + \frac{1}{2}(\gamma - \gamma_0)^2V''(\gamma_0) + O[(\gamma - \gamma_0)^3], \tag{37}$$

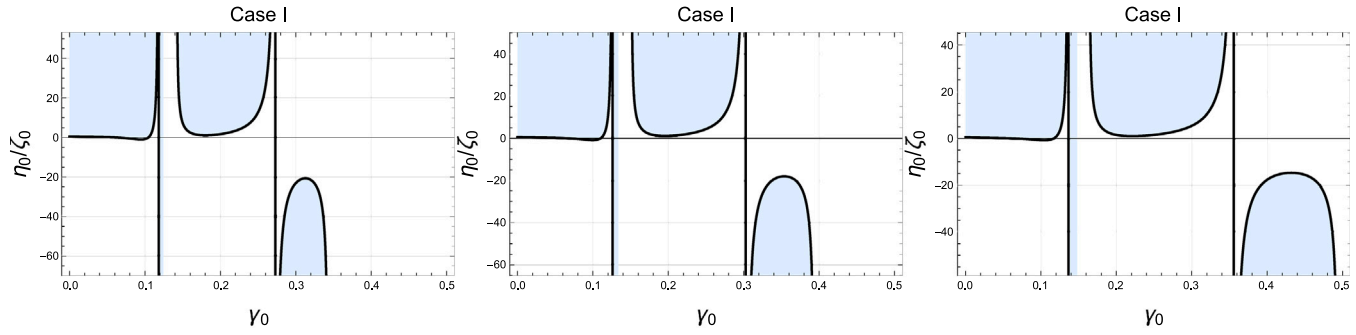

Fig. 15. Stable regions for case (i) for different values of ω as $\omega = 0.3$ (first plot), $\omega = 0.4$ (second plot), $\omega = 0.5$ (third plot). The straight line shows the position of the expected event horizon of the developed structure. Stable regions are denoted with shaded regions.

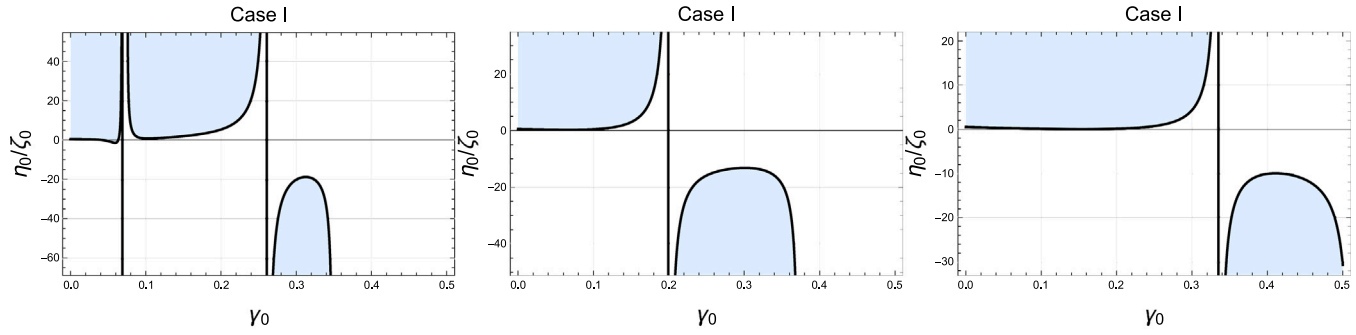

Fig. 16. Stable regions for case i for different values of ω as $W_0 = 0.1$ (first plot), $W_0 = 0.4$ (second plot), $W_0 = 0.6$ (third plot).

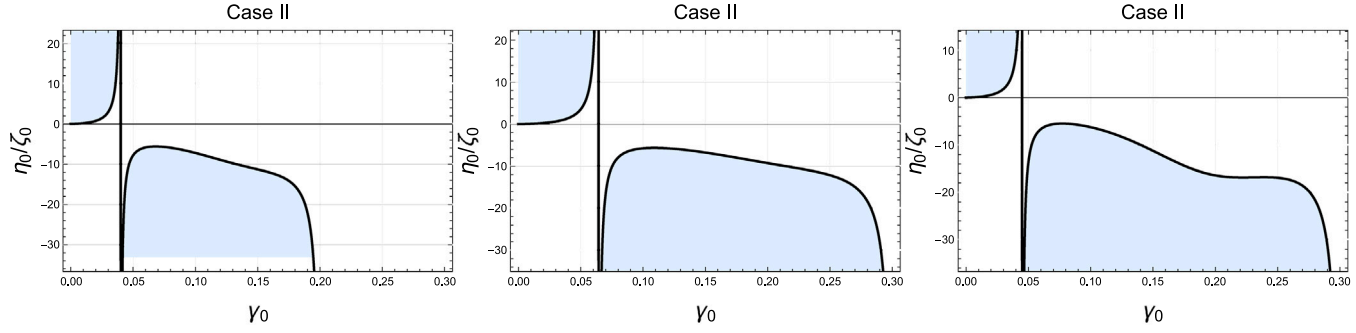

Fig. 17. Stable regions for case ii for different values of ω as $m = 0.5$ (first plot), $m = 0.7$ (second plot), $m = 1$ (third plot).

which leads to

$$V(\gamma) = \frac{1}{2}(\gamma - \gamma_0)^2 V''(\gamma_0). \tag{38}$$

Also, we have

$$M(\gamma_0) = 4\pi\gamma_0^2\sigma_0, \qquad M'(\gamma_0) = -8\pi\gamma_0 p_0, \quad M''(\gamma_0) = -8\pi p_0 + 16\pi\xi_0^2(\sigma_0 + p_0),$$

with $\xi_0^2 = dp/d\sigma|_{\gamma=\gamma_0}$ is a EoS parameter. Hence, we obtain:

$$\begin{aligned} V''(\gamma_0) = & -\frac{1}{2\gamma_0^4 M^4}\left\{-\gamma_0^4 M(2m - b(\gamma_0))\left(M''(2m - b(\gamma_0)) - 4M'b'(\gamma_0)\right)\right. \\ & + \gamma_0^4 M^2\left((b(\gamma_0) - 2m)b''(\gamma_0) + b'(\gamma_0)^2\right) \\ & + \gamma_0 M^4\left(\gamma_0\left(\gamma_0 b''(\gamma_0) - 2b'(\gamma_0) + \left(M'\right)^2\right) + 2b(\gamma_0) + 4m\right) \\ & + 3\gamma_0^4\left(M'\right)^2(b(\gamma_0) - 2m)^2 \\ & \left. + \gamma_0 M^5\left(\gamma_0 M'' - 4M'\right) + 3M^6\right\}. \end{aligned} \tag{39}$$

For stable configuration, we can obtain

$$\begin{aligned} & -\left(-\sigma_0(2m - b(\gamma_0))\left(32\pi\gamma_0 p_0 b'(\gamma_0) + (2m - b(\gamma_0))(16\pi\xi_0^2(p_0 + \sigma_0) - 8\pi p_0)\right)\right. \\ & +48\pi p_0^2(b(\gamma_0) - 2m)^2 \\ & +4\pi\gamma_0^2\sigma_0^2\left((b(\gamma_0) - 2m)b''(\gamma_0) + b'(\gamma_0)^2\right) \\ & +64\pi^3\gamma_0^3\sigma_0^4\left(\gamma_0^2 b''(\gamma_0) - 2\gamma_0 b'(\gamma_0) + 2b(\gamma_0) + 64\pi^2\gamma_0^3 p_0^2 + 4m\right) \\ & \left.+2048\pi^5\gamma_0^6\sigma_0^5((2\xi_0^2 + 3)p_0 + 2\xi_0^2\sigma_0) + 3072\pi^5\gamma_0^6\sigma_0^6\right)(128\pi^3\gamma_0^6\sigma_0^4)^{-1} > 0, \end{aligned} \tag{40}$$

It can be further characterized as

$$V''(\gamma_0) > 0, \quad \Rightarrow \quad \zeta(\gamma_0)\xi_0^2 - \eta_0 > 0. \tag{41}$$

Here, the coefficient of the EoS parameter is denoted with $\zeta(\gamma_0) = \zeta_0$ and remaining terms are named as $\eta(\gamma_0)\eta_0$.

The stable configuration can be obtained from the following constraints:

- **(i)** For $\zeta_0 < 0 \Rightarrow \quad \xi_0^2 < \eta_0/\zeta_0$:
- **(ii)** For $\zeta_0 > 0 \Rightarrow \xi_0^2 > \eta_0/\zeta_0$,

where

$$\begin{aligned} \eta_0 = & \, b(\gamma_0)\left(8\left(mp_0(6p_0 + \sigma_0) - 4\pi^2\gamma_0^3\sigma_0^4\right) - \gamma_0\sigma_0\left(\gamma_0\sigma_0 b''(\gamma_0) + 8p_0 b'(\gamma_0)\right)\right) \\ & + \gamma_0\sigma_0\left(2\gamma_0\sigma_0 b''(\gamma_0)\left(m - 8\pi^2\gamma_0^3\sigma_0^2\right)\right. \end{aligned}$$

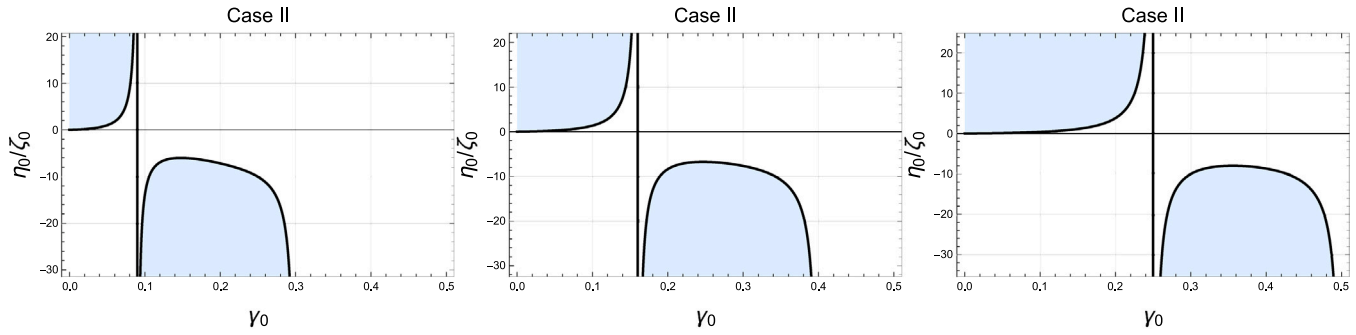

Fig. 18. Stable regions for case ii for different values of ω as $r_0 = 0.1$ (first plot), $r_0 = 0.4$ (second plot), $r_0 = 0.6$ (third plot).

$$
\begin{aligned}
&+\ b'(\gamma_0)\left(-\gamma_0\sigma_0 b'(\gamma_0) + 32\pi^2\gamma_0^3\sigma^3 + 16mp_0\right)\Big)\\
&-\ 2p_0 b(\gamma_0)^2(6p_0+\sigma_0) - 8\left(32\pi^4\gamma_0^6\sigma_0^4\left(4p_0^2+6p_0\sigma_0+3\sigma_0^2\right)\right. \qquad (42)\\
&+\ \left.8\pi^2\gamma_0^3 m\sigma_0^4 + m^2 p_0(6p_0+\sigma_0)\right),\\
\zeta_0 &= 4\sigma_0(p_0+\sigma_0)\left(4mb(\gamma_0) - b(\gamma_0)^2 + 256\pi^4\gamma_0^6\sigma_0^4 - 4m^2\right).
\end{aligned}
$$

We consider these two cases of shape functions given as:

$$
\begin{aligned}
b_1(\gamma_0) &= -\frac{\gamma_0^5}{\gamma_0^4 + W_0^4(W_0-\omega)} + \gamma_0 + \omega,\\
b_2(\gamma_0) &= \gamma_0 - \gamma_0^{3-2m}\left(\gamma_0^m - r_0^m\right)^{2-\frac{2}{m}}.
\end{aligned}
$$

- We observe the impact of physical parameters on the stable configurations of the developed thin-shell around the WH structure as shown in Figs. 15–18. For the first case, we observe that the shape function parameter greatly affects the stable regions of the shell. Also, the massive BH plays a remarkable role in maintaining the shell's stable configuration.

9. Conclusion

In this study, we study the modified $F(T,T_G)$ gravity model, an extension of teleparallel gravity incorporating the torsional invariant T_G, introduced to construct a teleparallel equivalent of the Gauss–Bonnet term. Through detailed derivations, we examined the teleparallel invariants, torsion tensors, and modified field equations resulting from this framework. Where the geometry of wormhole (WH) solutions was analyzed under the modified gravity context, considering conditions for shape and redshift functions, as well as the violation of energy conditions. Also, the anisotropic stress–energy tensor with its interplay of radial and tangential pressures was incorporated to characterize the material composition of WHs. These investigations reveal the structure of $F(T,T_G)$ gravity and its applications in cosmology and astrophysics, particularly for traversable wormholes and energy conditions.

The present study investigates $F(T,T_G)$ gravity, focusing on two distinct and highly inclusive embedded wormhole (WH) solutions. The newly proposed embedded shape functions are considered the most optimal options and satisfy the Morris and Thorne WH criteria. Moreover, we investigated the influence of dark matter (DM) halos on URC, NFW, and SFDM profiles within the context of the energy conditions case of $F(T,T_G)$ gravity framework. The shape functions studied fulfill all required criteria for the presence of WH structures in the presence of DM. The primary findings of this study can be summarized as follows:

- Figs. 1 and 8 show the energy density, represented as ρ, for the URC, NFW, and SFDM distributions within the framework of $F(T,T_G)$ gravity, as well as for the two $F(T,T_G)$ gravity models. It is observed that the energy density stays non-negative in all wormhole (WH) designs, except for the SFDM matter profile at small radial distances l.
- Figs. 2 and 9 illustrate the important energy condition, represented as $\rho + p_r$, for embedded wormhole (WH) solutions in both variations of $F(T,T_G)$ gravity. In the second model of $F(T,T_G)$ gravity, the negativity of $\rho + p_r$ can be observed, while in the first model it is only seen for $F(T,T_G)$ gravity and scalar field dark matter (SFDM). Exotic matter is detected when the sum of density and radial pressure has a negative nature. Since exotic matter is essential for making a wormhole, the outcomes of this study, which involve embedded solutions for WH, are both possible and physically plausible.
- The Weak Energy Condition (WEC), shown as $\rho + p_t$, is depicted in Figs. 4 and 5 (first model) and Figs. 11 and 12 (second model) under the framework of $F(T,T_G)$ gravity. The Strong Energy Condition (SEC), represented by $\rho+p_r+2p_2$, is shown in Figs. 6 and 12 for the identical gravitational model. Moreover, it has been observed that in specific areas of the wormhole (WH) setups, this characteristic displays negative values.
- Figs. 7 and 14 exhibit negative values in specific radial distance intervals l, as illustrated by the graphical representation of the trace energy condition $(\rho - p_r - 2p_2)$.
- We studied two specific models of $F(T,T_G)$ gravity to investigate the physical viability of wormhole (WH) solutions under varying parameter constraints. For the first model, $F(T,T_G) = \Psi_1\left(-\frac{\Psi_3 T_G}{\sqrt{T}}\right)^{\Psi_2}$, we established that physically meaningful solutions require $\Psi_2 = 1$, with positive values of Ψ_1 and Ψ_3 confined to the range $(0,1)$. In the second equation, $F(T,T_G) = \Psi_1(\Psi_2 T_G + T^2) + \Psi_3(\Psi_4 T_G + T^2)^2 - T$, it is also required that $\Psi_2 = 1$, with small positive values of Ψ_3 and Ψ_4 for physical validity. The figures explain the energy density (ρ), radial pressure (p_r), and tangential pressure (p_t) for profiles like URC, CDM halo with NFW, and SFDM, confirming compliance with energy conditions. These results show the potential of $F(T,T_G)$ gravity to support wormhole structures and explain exotic spacetime formations.
- The stable configurations of the generated thin-shell surrounding the WH structure are impacted by physical parameters, as illustrated in Figs. 15–18. We find that in the first scenario, the stable portions of the shell are significantly influenced by the shape function parameter. The massive BH also contributes significantly to the shell's stable structure.

We explored embedded wormhole (WH) solutions through two different methods, concentrating on the Karmarkar criterion and the generalized Ellis–Bronnikov spacetime. Using the Karmarkar condition within class-I Riemannian embeddings, we established important equations controlling the geometry of embedded WHs, yielding particular solutions such as the embedded shape function. The next method focused on the extremely static Ellis–Bronnikov WH model, known for its absence of horizons and geometrical features linked to radial distance and proper radial coordinate. Analytical findings showed a relationship between the radial coordinate and proper distance via

embedding equations, allowing for the examination of WH properties with varying parameter setups. Where numerical analysis and graphical representations illustrated the characteristics of energy density (ρ), radial pressure (p_r), tangential pressure (p_t), and their mixtures in different situations, such as $F(T,T_G)$ gravity, the URC profile, the CDM halo with the NFW profile, and the SFDM profile. These results offer a more thorough understanding of the geometric and physical traits of embedded WH solutions, illustrating their reliance on particular parameters and gravitational profiles.

This research investigates how URC, NFW, and SFDM dark matter profiles affect wormhole solutions within the context of $F(T,T_G)$ gravity. Embedding these profiles as energy density functions in the analysis emphasizes their influence on energy conditions such as NEC, WEC, SEC, and TEC. The results illustrate energy conditions, especially related to the SFDM profile, where negative energy densities are seen at short radial distances. Moreover, breaches in NEC are seen in all profiles, where the importance of exotic matter in maintaining wormhole structures inside dark matter halos is. The results explain the important interaction between the distribution of dark matter density and the energy limitations that control traversable wormholes.

CRediT authorship contribution statement

Asifa Ashraf: Writing – review & editing, Writing – original draft, Visualization, Validation, Software, Methodology, Investigation, Formal analysis, Conceptualization. **Wen-Xiu Ma:** Writing – review & editing, Writing – original draft, Visualization, Validation, Investigation, Formal analysis, Conceptualization. **Faisal Javed:** Writing – review & editing, Writing – original draft, Visualization, Validation, Methodology, Formal analysis, Conceptualization. **S.K. Maurya:** Writing – review & editing, Writing – original draft, Visualization, Investigation, Formal analysis, Conceptualization. **Farruh Atamurotov:** Writing – review & editing, Writing – original draft, Visualization, Formal analysis, Conceptualization. **Abdelmalek Bouzenada:** Writing – review & editing, Writing – original draft, Visualization, Validation, Formal analysis, Conceptualization. **Magda Abd El-Rahman:** Conceptualization, Formal analysis, Visualization, Writing – original draft, Writing – review & editing.

Declaration of competing interest

The authors declare that they have no known competing financial interests or personal relationships that could have appeared to influence the work reported in this paper.

Acknowledgments

Magda Abd El-Rahman extends their appreciation to the Deanship of Research and Graduate Studies at King Khalid University for funding this work through Large Research Project under grant number RGP2/81/45.

Appendix A

$$
\begin{aligned}
\chi_1 &= -\left(3b'(r)+2\right)\lambda'(r)+2r\lambda''(r)+2r\lambda'(r)^2,\\
\chi_2 &= \frac{\Psi_3\left(2r^2b'(r)\lambda'(r)+b(r)^2\left(-2r\lambda''(r)-2r\lambda'(r)^2+3\lambda'(r)\right)+r\chi_1 b(r)\right)}{r^5\sqrt{\frac{(r-b(r))^2\lambda'(r)}{r^5}}},\\
\chi_3 &= \frac{\Psi_2\left(\Psi_2+2\right)r^2\left(\left(5b(r)-r\left(2b'(r)+3\right)\right)\lambda'(r)+r(r-b(r))\lambda''(r)\right)}{(r-b(r))^2\lambda'(r)^2},\\
\chi_4 &= 2rb''(r)\lambda'(r)-3b'(r)^2\lambda'(r)+2b'(r)\left(2r\lambda''(r)+r\lambda'(r)^2-4\lambda'(r)\right),\\
\chi_5 &= -\lambda'(r)\left(4r^2\lambda''(r)+15\right)+8r\lambda'(r)^2+r\left(11\lambda''(r)-2r\lambda^{(3)}(r)\right),\\
\chi_6 &= -3rb''(r)+18b'(r)+4r^2\lambda''(r)+8,\\
\chi_7 &= -2r\left(2b'(r)+3\right)\lambda'(r)^2+r\left(2r\lambda^{(3)}(r)-\left(7b'(r)+8\right)\lambda''(r)\right)+\chi_6\lambda'(r),\\
\chi_8 &= r\chi_7 b(r)+\chi_5 b(r)^2+r^2\chi_4,\\
\chi_9 &= 2r^2b'(r)\lambda'(r)+b(r)^2\left(-2r\lambda''(r)-2r\lambda'(r)^2+3\lambda'(r)\right)+r\chi_1 b(r),\\
\chi_{10} &= r\left(2r\lambda^{(4)}(r)-\lambda^{(3)}(r)\left(11b'(r)+14\right)\right)\\
&\quad+2\lambda''(r)\left(-5rb''(r)+34b'(r)+20\right)+4r^2\lambda''(r)^2,\\
\chi_{11} &= 3r^2b^{(3)}(r)-30rb''(r)+8b'(r)\left(2r^2\lambda''(r)+15\right)\\
&\quad-4r^3\lambda^{(3)}(r)+24r^2\lambda''(r)+40,\\
\chi_{12} &= -4r\lambda'(r)^2\left(rb''(r)-8b'(r)-6\right)-\chi_{11}\lambda'(r)+r\chi_{10},
\end{aligned}
$$

$$
\begin{aligned}
\chi_{13} &= 2r^2\lambda^{(4)}(r)+4r^2\lambda''(r)^2-19r\lambda^{(3)}(r)+70\lambda''(r),\\
\chi_{14} &= \lambda'(r)\left(4r^3\lambda^{(3)}(r)-32r^2\lambda''(r)-90\right)+40r\lambda'(r)^2+r\chi_{13},\\
\chi_{15} &= \lambda'(r)\left(-9rb''(r)+8r^2\lambda''(r)+40\right)\\
&\quad-12r\lambda'(r)^2+2r\left(3r\lambda^{(3)}(r)-14\lambda''(r)\right),\\
\chi_{16} &= 3rb''(r)\lambda''(r)+rb''(r)\lambda'(r)^2+\left(rb^{(3)}(r)-7b''(r)\right)\lambda'(r),\\
\chi_{17} &= -2b'(r)^2\left(5r\lambda''(r)+2r\lambda'(r)^2-15\lambda'(r)\right)+\chi_{15}b'(r)+2r\chi_{16},\\
\chi_{18} &= \chi_9\left(r\chi_{12}b(r)-\chi_{14}b(r)^2+r^2\chi_{17}\right)+\left(\Psi_2-2\right)\chi_8^2,\\
\chi_{19} &= -8r^2b'(r)\lambda'(r)+4rb(r)\left(\left(3b'(r)+2\right)\lambda'(r)-2r\lambda''(r)-2r\lambda'(r)^2\right)\\
&\quad+4b(r)^2\left(2r\lambda''(r)+2\right.\\
&\quad\left.\times r\lambda'(r)^2-3\lambda'(r)\right),\\
\chi_{20} &= \frac{8\left(\Psi_2-1\right)\Psi_2\chi_8(r-b(r))\left(r\left(3b'(r)+2\right)-3b(r)\right)}{r\chi_9^2},\\
\chi_{21} &= \frac{\Psi_2r^2(r(2\lambda(r)-1)-2b(r)(\lambda(r)-1))}{(r-b(r))^2\lambda'(r)}+8\Psi_2-8,
\end{aligned}
$$

$$
\begin{aligned}
\chi_{22} &= \frac{\Psi_2r^2\left(\lambda(r)\left(b'(r)+2r\right)-b'(r)-b(r)\left(2\lambda(r)^2+3\lambda(r)+1\right)+2r\lambda(r)^2+2r\right)}{(r-b(r))^2\lambda'(r)},\\
\chi_{23} &= \frac{16\left(\Psi_2-1\right)\Psi_2\chi_8(r-b(r))\lambda(r)\left(r^2\left(3b'(r)+2\lambda(r)+4\right)-b(r)(2r\lambda(r)+4r+3)\right)}{r^2\chi_9^2}.
\end{aligned}
$$

Appendix B

$$
\begin{aligned}
\zeta_1 &= \Psi_3\Psi_4r^9b'(r)^2\left(\Psi_4r^2\left(2r\left(-73rb(r)+41b(r)^2+32r^2\right)\lambda''(r)\right.\right.\\
&\quad+r\left(-56rb(r)+31b(r)^2+24r^2\right)\lambda'(r)^2\\
&\quad\left.\left.-\ 6\left(-71rb(r)+41b(r)^2+30r^2\right)\lambda'(r)\right)-80(2r-3b(r))(r-b(r))^2\lambda'(r)^2\right),\\
\zeta_2 &= -3r^2\left(-16rb(r)+15b(r)^2+4r^2\right)\lambda'(r)\\
&\quad+4r^3\left(-5rb(r)+4b(r)^2+r^2\right)\lambda''(r)-2\left(\left(5r^2+14\right)r^2b(r)\right.\\
&\quad\left.-\left(5r^2+16\right)rb(r)^2+6b(r)^3-4r^3\right)\lambda'(r)^2,\\
\zeta_3 &= (r-b(r))\lambda'(r)\left(8r^2\left(-3rb''(r)+2r^2\lambda''(r)+12\right)\right.\\
&\quad+rb(r)\left(27rb''(r)-56r^2\lambda''(r)-404\right)+b(r)^2\\
&\quad\left.\times\ \left(38r^2\lambda''(r)+339\right)\right)+2r\left(-10rb(r)+7b(r)^2+3r^2\right)\lambda^{(3)}(r)\\
&\quad+2r(r-b(r))\left(121rb(r)-95b(r)^2-32r^2\right)\\
&\quad\times\lambda''(r)+2r^2b(r)\left(-5rb(r)+3b(r)^2+2r^2\right)\lambda'(r)^3\\
&\quad+r\left(144r^2b(r)-208rb(r)^2+91b(r)^3-28r^3\right)\lambda'(r)^2,\\
\zeta_4 &= -80\Psi_1r^{10}(r-b(r))^2\lambda'(r)\\
&\quad+16\Psi_3\left(-8\Psi_4\zeta_2r^3(r-b(r))^2\lambda'(r)-1664(r-b(r))^6\lambda'(r)^3+\Psi_4^2\zeta_3r^7\right)+r^{15},\\
\zeta_5 &= r^3(r-b(r))\lambda''(r)+r^2(5b(r)-3r)\lambda'(r)+(r-b(r))^2\lambda'(r)^2,\\
\zeta_6 &= 48\lambda'(r)^2\left(21r^2\lambda''(r)-93r\lambda'(r)+28\lambda'(r)^2\right)\\
&\quad+\Psi_4r^3\left(2r^3\lambda''(r)^2-2\left(5r^2+14\right)\lambda'(r)^3+r\lambda'(r)^2\right.\\
&\quad\left.\times\ \left(2\left(r^2+10\right)\lambda''(r)+15\right)-13r^2\lambda'(r)\lambda''(r)+20r\lambda'(r)^4\right),\\
\zeta_7 &= 2\left(\Psi_4r^4+168\right)\lambda'(r)^2+2r^2\left(\Psi_4r^2+84\right)\lambda''(r)-3r\left(\Psi_4r^2+264\right)\lambda'(r),\\
\zeta_8 &= \zeta_8=2r\left(\left(24-11rb''(r)\right)\lambda''(r)+2r^2\lambda''(r)^2+r\left(r\lambda^{(4)}(r)-8\lambda^{(3)}(r)\right)\right)\\
&\quad+2r\left(15-4rb''(r)\right)\lambda'(r)^2\\
&\quad+\lambda'(r)\left(-7r^2b^{(3)}(r)+66rb''(r)+4r^3\lambda^{(3)}(r)-28r^2\lambda''(r)-48\right),
\end{aligned}
$$

$$
\begin{aligned}
\zeta_9 &= \zeta_9 = \Psi_4^2\zeta_8 r^5 - 384\lambda'(r)^2\left(7r^2\lambda''(r) - 23r\lambda'(r) + 4\lambda'(r)^2\right)\\
&\quad - 16\Psi_4 r^3\left(r^3\lambda''(r)^2 - \left(3r^2+2\right)\lambda'(r)^3\right.\\
&\quad \left. + r\lambda'(r)^2\left(\left(r^2+2\right)\lambda''(r) + 3\right) - 4r^2\lambda'(r)\lambda''(r) + 2r\lambda'(r)^4\right),\\
\zeta_{10} &= 3\Psi_4^2 r^7 b''(r)\lambda''(r) + \lambda'(r)^2\left(\Psi_4^2 r^7 b''(r) + 192r^2\lambda''(r)\right)\\
&\quad + \Psi_4^2 r^6\left(rb^{(3)}(r) - 8b''(r)\right)\lambda'(r)\\
&\quad - 576r\lambda'(r)^3 + 96\lambda'(r)^4,
\end{aligned}
$$

$$
\begin{aligned}
\zeta_{11} &= 7680\lambda'(r)^2\left(7r^2\lambda''(r) - 29r\lambda'(r) + 7\lambda'(r)^2\right)\\
&\quad + 32\Psi_4 r^3\left(8r^3\lambda''(r)^2 - 4\left(9r^2+13\right)\lambda'(r)^3 + r\lambda'(r)^2\right.\\
&\quad \left.\times\left(8\left(r^2+5\right)\lambda''(r) + 49\right) - 47r^2\lambda'(r)\lambda''(r) + 40r\lambda'(r)^4\right)\\
&\quad + \Psi_4^2 r^5\left(4r^3\lambda'(r)^4 - 12r^2\lambda'(r)^3 + r\lambda'(r)^2\right.\\
&\quad \left.\times\left(8r^2\lambda''(r) - 199\right) - 2r\left(4r^2\lambda^{(4)}(r) + 6r^2\lambda''(r)^2 - 44r\lambda^{(3)}(r) + 173\lambda''(r)\right)\right.\\
&\quad \left. + \lambda'(r)\left(-16r^3\lambda^{(3)}(r)\right.\right.\\
&\quad \left.\left. + \ 140r^2\lambda''(r) + 450\right)\right),\\
\zeta_{12} &= \Psi_4^2 r^5\left(4r\lambda'(r)^2\left(2rb''(r) + 2r^2\lambda''(r) - 65\right)\right.\\
&\quad \left. + r\left(\left(20rb''(r) - 439\right)\lambda''(r) - 20r^2\lambda''(r)^2 - 12r\right.\right.\\
&\quad \left.\left. + \ \left(r\lambda^{(4)}(r) - 10\lambda^{(3)}(r)\right)\right)\right.\\
&\quad \left. + \lambda'(r)\left(6r^2 b^{(3)}(r) - 69rb''(r) - 24r^3\lambda^{(3)}(r) + 198r^2\lambda''(r) + 539\right)\right.\\
&\quad \left. + \ 4r^3\lambda'(r)^4 - 10r^2\lambda'(r)^3\right) + 768\lambda'(r)^2\left(35r^2\lambda''(r) - 135r\lambda'(r) + 28\lambda'(r)^2\right)\\
&\quad + 16\Psi_4 r^3\left(12r^3\lambda''(r)^2\right.\\
&\quad \left. - 48\left(r^2+1\right)\lambda'(r)^3 + r\lambda'(r)^2\left(4\left(3r^2+10\right)\lambda''(r) + 59\right)\right.\\
&\quad \left. - \ 63r^2\lambda'(r)\lambda''(r) + 40r\lambda'(r)^4\right),\\
\zeta_{13} &= \Psi_4^2 r^5\left(4r\lambda'(r)^2\left(5rb''(r) + r^2\lambda''(r) - 55\right)\right.\\
&\quad \left. - 2r\left(\left(181 - 26rb''(r)\right)\lambda''(r) + 11r^2\lambda''(r)^2 + 6r\left(r\lambda^{(4)}(r)\right.\right.\right.\\
&\quad \left.\left.\left. - \ 9\lambda^{(3)}(r)\right)\right) + \lambda'(r)\left(16r^2 b^{(3)}(r) - 169rb''(r) - 24r^3\lambda^{(3)}(r) + 184r^2\lambda''(r) + 410\right)\right.\\
&\quad \left. + 2r^3\lambda'(r)^4 - 4r^2\right.\\
&\quad \left.\times\ \lambda'(r)^3\right) + 768\lambda'(r)^2\left(21r^2\lambda''(r) - 75r\lambda'(r) + 14\lambda'(r)^2\right)\\
&\quad + 16\Psi_4 r^3\left(8r^3\lambda''(r)^2 - 2\left(14r^2+11\right)\lambda'(r)^3\right.\\
&\quad \left. + \ r\lambda'(r)^2\left(4\left(2r^2+5\right)\lambda''(r) + 31\right) - 37r^2\lambda'(r)\lambda''(r) + 20r\lambda'(r)^4\right),\\
\zeta_{14} &= 4\zeta_9 r^7 b(r) + 2\zeta_{13} r^6 b(r)^2 - 2\zeta_{12} r^5 b(r)^3 + \zeta_{11} r^4 b(r)^4 - 32\zeta_6 r^3 b(r)^5\\
&\quad + 64\zeta_7 r^2 b(r)^6\lambda'(r)^2 - 1536rb(r)^7\\
&\quad \times\lambda'(r)^2\left(r^2\lambda''(r) - 5r\lambda'(r) + 4\lambda'(r)^2\right) + 768b(r)^8\lambda'(r)^4 + 8\zeta_{10} r^8,
\end{aligned}
$$

$$
\begin{aligned}
\zeta_{15} &= 8\Psi_3\left(\lambda'(r)\left(\Psi_4\left(-r^5\right)(2r - 3b(r))\left(rb'(r) - b(r)\right)\right.\right.\\
&\quad \left.\left. - \ 2(r - b(r))\left(\Psi_4 r^6 b(r) - 8(r - b(r))^3\right)\lambda'(r)\right)\right.\\
&\quad \left. + \ 2\Psi_4 r^6 b(r)(b(r) - r)\lambda''(r)\right) + \Psi_1 r^{10},\\
\zeta_{16} &= \lambda'(r)\left(\Psi_2 r^5(2r - 3b(r))\left(rb'(r) - b(r)\right)\right.\\
&\quad \left. + \ 2(r - b(r))\left(\Psi_2 r^6 b(r) - 8(r - b(r))^3\right)\lambda'(r)\right) + 2\Psi_2 r^6\\
&\quad \times(r - b(r))b(r)\lambda''(r),\\
\zeta_{17} &= \Psi_4\left(-r^5\right)(2r - 3b(r))\left(rb'(r) - b(r)\right)\\
&\quad - 2(r - b(r))\left(\Psi_4 r^6 b(r) - 8(r - b(r))^3\right)\lambda'(r),\\
\zeta_{18} &= \lambda'(r)\left((2r - 3b(r))\left(rb'(r) - b(r)\right) + 2r(r - b(r))b(r)\lambda'(r)\right)\\
&\quad + 2r(r - b(r))b(r)\lambda''(r),\\
\zeta_{19} &= \lambda'(r)\left(\Psi_4\left(-r^5\right)(2r - 3b(r))\left(rb'(r) - b(r)\right)\right.\\
&\quad \left. - \ 2(r - b(r))\left(\Psi_4 r^6 b(r) - 8(r - b(r))^3\right)\lambda'(r)\right)\\
&\quad + 2\Psi_4 r^6 b(r)(b(r) - r)\lambda''(r),\\
\zeta_{20} &= -\lambda'(r)\left(4r^2\lambda''(r) + 15\right) + 8r\lambda'(r)^2 + r\left(11\lambda''(r) - 2r\lambda^{(3)}(r)\right),\\
\zeta_{21} &= 192r^2\left(4rb'(r)\lambda''(r) + \lambda'(r)\left(2rb''(r) + b'(r)\left(-3b'(r) + 2r\lambda'(r) - 8\right)\right)\right.\\
&\quad + rb(r)\left(-2r\left(2b'(r)+3\right)\lambda'(r)^2\right.\\
&\quad \left. + r\left(2r\lambda^{(3)}(r) - \left(7b'(r)+8\right)\lambda''(r)\right)\right.
\end{aligned}
$$

$$
\begin{aligned}
&\quad \left. + \ \lambda'(r)\left(-3rb''(r) + 18b'(r) + 4r^2\lambda''(r) + 8\right)\right) + \zeta_{20} b(r)^2,\\
\zeta_{22} &= -16\Psi_3\left(2\Psi_4 r^6 b(r)(b(r) - r)\lambda''(r) + \zeta_{17}\lambda'(r)\right)^2\\
&\quad + 4\Psi_1\zeta_{16} r^{10} - 4\zeta_{18} r^5\left(8\Psi_3\Psi_4\zeta_{19} + \Psi_1\Psi_2 r^{10}\right),\\
\zeta_{23} &= r\left(2r\lambda^{(4)}(r) - \lambda^{(3)}(r)\left(11b'(r) + 14\right)\right)\\
&\quad + 2\lambda''(r)\left(-5rb''(r) + 34b'(r) + 20\right) + 4r^2\lambda''(r)^2,
\end{aligned}
$$

$$
\begin{aligned}
\zeta_{24} &= 4r\lambda'(r)^2\left(-rb''(r) + 8b'(r) + 6\right) - \lambda'(r)\left(8b'(r)\left(2r^2\lambda''(r) + 15\right)\right.\\
&\quad \left. + r\left(r\left(3b^{(3)}(r) - 4r\lambda^{(3)}(r)\right.\right.\right.\\
&\quad \left.\left.\left. + \ \ 24\lambda''(r)\right) - 30b''(r)\right) + 40\right) + \zeta_{23} r,\\
\zeta_{25} &= r^2\left(-2b'(r)^2\left(5r\lambda''(r) + \lambda'(r)\left(2r\lambda'(r) - 15\right)\right)\right.\\
&\quad \left. + 2r\left(rb^{(3)}(r)\lambda'(r) + b''(r)\left(3r\lambda''(r) + \lambda'(r)\left(r\lambda'(r) - 7\right)\right)\right)\right.\\
&\quad \left. + b'(r)\left(\lambda'(r)\left(-9rb''(r) + 8r^2\lambda''(r) + 40\right) - 12r\lambda'(r)^2 + 2r\left(3r\lambda^{(3)}(r) - 14\lambda''(r)\right)\right)\right)\\
&\quad - b(r)^2\left(r\left(2r^2\lambda^{(4)}(r)\right.\right.\\
&\quad \left.\left. + \ 4r^2\lambda''(r)^2 - 19r\lambda^{(3)}(r) + 70\lambda''(r)\right) + \lambda'(r)\left(4r^2\left(r\lambda^{(3)}(r) - 8\lambda''(r)\right) - 90\right)\right.\\
&\quad \left. + 40\ r\lambda'(r)^2\right) + \zeta_{24} rb(r),\\
\zeta_{26} &= r^2\left(4rb'(r)\lambda''(r) + \lambda'(r)\left(2rb''(r) + b'(r)\left(-3b'(r) + 2r\lambda'(r) - 8\right)\right)\right.\\
&\quad \left. + rb(r)\left(-2r\left(2b'(r)+3\right)\lambda'(r)^2 + r\right.\right.\\
&\quad \left.\left. \times\ \left(2r\lambda^{(3)}(r) - \left(7b'(r)+8\right)\lambda''(r)\right) + \lambda'(r)\left(-3rb''(r) + 18b'(r) + 4r^2\lambda''(r) + 8\right)\right)\right.\\
&\quad \left. + \zeta_{20} b(r)^2,\right.\\
\zeta_{27} &= \zeta_{26}(\lambda(r) - 1)b'(r) - b(r)(\lambda(r) + 1)(2\lambda(r) + 1) + 2r\left(\lambda(r)^2 + \lambda(r) + 1\right),\\
\zeta_{28} &= 8\Psi_3\left(\lambda'(r)\left(\Psi_4\left(-r^5\right)(2r - 3b(r))\left(rb'(r) - b(r)\right)\right.\right.\\
&\quad \left.\left. - \ 2(r - b(r))\left(\Psi_4 r^6 b(r) - 24(r - b(r))^3\right)\lambda'(r)\right)\right.\\
&\quad \left. + 2\Psi_4 r^6 b(r)(b(r) - r)\lambda''(r)\right) + \Psi_1 r^{10},\\
\zeta_{29} &= -32\zeta_{28} r^2(r - b(r))^2(\lambda(r) - 1)\left(\left(5b(r) - r\left(2b'(r) + 3\right)\right)\lambda'(r) + r(r - b(r))\lambda''(r)\right)\\
&\quad - 16\Psi_3\left(2\Psi_4 r^6\right.\\
&\quad \left.\times\ b(r)(b(r) - r)\lambda''(r) + \zeta_{17}\lambda'(r)\right)^2 + 4\Psi_1\zeta_{16} r^{10},\\
\zeta_{30} &= \zeta_{29} + \zeta_{27} r^{17}\left(\frac{16\zeta_{15}(r - b(r))^2\lambda'(r)}{r^{15}} - 1\right).
\end{aligned}
$$

Data availability

No data was used for the research described in the article.

References

[1] L. Flamm, Phys. Z 17 (1916) 448.
[2] A. Einstein, N. Rosen, Phys. Rev. 48 (1935) 73.
[3] C.W. Misner, J.A. Wheeler, Ann. Phys. 2 (1957) 525.
[4] H.G. Ellis, J. Math. Phys. 14 (1973) 104.
[5] K.A. Bronnikov, Acta Phys. Pol. B 4 (1973) 251.
[6] G. Clement, Gen. Relativity Gravitation 16 (1984) 131.
[7] M.S. Morris, K.S. Thorne, Am. J. Phys. 56 (1988) 395.
[8] M.G. Richarte, C. Simeone, Phys. Rev. D 76 (2007) 087502.
[9] E.F. Eiroa, M.G. Richarte, C. Simeone, Phys. Lett. A 373 (2008) 1–4.
[10] M. Sharif, F. Javed, Gen. Relativity Gravitation 48 (2016) 158; Ann. Phys. 407 (2019) 198; Chin. J. Phys. 61 (2019) 262; Astrophys Space. Sci. 366 (2021) 103; Eur. Phys. J. C 81 (2021) 47.
[11] S. Perlmutter, et al., Nature 391 (1998) 51.
[12] S. Perlmutter, et al., Astrophys. J. 517 (1999) 565.
[13] T.P. Sotiriou, V. Faraoni, Rev. Modern Phys. 82 (2010) 451.
[14] G. Cognola, et al., Phys. Rev. D 73 (2006) 084007.
[15] T. Harko, F.S.N. Lobo, S. Nojiri, S.D. Odintsov, Phys. Rev. D. 84 (2011) 024020.
[16] Y. Fujii, K. Maeda, Cambridge University Press, 2004.
[17] S. Capozziello, et al., Phys. Rev. D 86 (2012) 127504.
[18] S. Capozziello, et al., Ann. Phys. 390 (2018) 303.
[19] S. Capozziello, R. Pincak, E. Bartos, Symmetry 12 (2020) 774.
[20] S. Capozziello, M. Francaviglia, Gen. Relativity Gravitation 40 (2008) 357.
[21] S. Capozziello, et al., Phys. Lett. B 639 (2006) 135.
[22] S. Capozziello, V.F. Cardone, A. Troisi, Phys. Rev. D 71 (2005) 043503.
[23] S. Capozziello, A. Stabile, A. Troisi, Classical Quantum Gravity 24 (2007) 2153.

[24] G. Kofinas, G. Leon, E.N. Saridakis, Classical Quantum Gravity 31 (2014) 175011.
[25] G. Kofinas, E.N. Saridakis, Phys. Rev. D 90 (2014) 084044.
[26] A. Jawad, Eur. Phys. J. Plus 130 (2015) 94.
[27] M. Zubair, A. Jawad, Astrophys. Space Sci. 360 (2015) 11.
[28] S. Chattopadhyay, et al., Astrophys. Space Sci. 353 (2014) 279–292.
[29] A.I. Keskin, Astrophys. Space Sci. 362 (2017) 50.
[30] M. Sharif, K. Nazir, Can. J. Phys. 95 (2017) 297–304.
[31] H.A. Buchdahl, Mon. Not. R. Astron. Soc. 150 (1) (1970) 1–8.
[32] S. Capozziello, M. Francaviglia, Gen. Relativity Gravitation 40 (2008) 357.
[33] S. Capozziello, S. Carloni, A. Troisi, Recent Res. Dev. Astron. Astrophys. 1 (2003) 625.
[34] T. Harko, F.S.N. Lobo, M.K. Mak, S.V. Sushkov, Phys. Rev. D 87 (2013) 067504.
[35] F. Rahaman, A. Banerjee, M. Jamil, A.K. Yadav, H. Idris, Internat. J. Theoret. Phys. 53 (2014) 1910.
[36] M. Jamil, F. Rahaman, R. Myrzakulov, P.K.F. Kuhfittig, N. Ahmed, U.F. Mondal, J. Korean Phys. Soc. 65 (2014) 917.
[37] K.A. Bronnikov, A.A. Starobinsky, JETP Lett. 85 (1) (2007) 1.
[38] K.A. Bronnikov, M.V. Skvortsova, A.A. Starobinsky, Gravit. Cosmol. 16 (3) (2010) 216–222.
[39] S. Bahamonde, M. Jamil, P. Pavlovic, M. Sossich, Phys. Rev. D 94 (2016) 044041.
[40] M.F. Shamir, I. Fayyaz, Eur. Phys. J. C 80 (2020) 1102.
[41] C.G. Böhmer, T. Harko, F.S.N. Lobo, Phys. Rev. D 85 (2012) 044033.
[42] M. Jamil, D. Momeni, R. Myrzakulov, Eur. Phys. J. C 73 (2013) 2267.
[43] G. Mustafa, et al., Int. J. Geom. Methods Mod. Phys. 16 (9) (2019) 1950143.
[44] A. Ashraf, et al., Mod. Phys. Lett. A. 35 (29) (2020) 2050240.
[45] M. Sharif, K. Nazir, Ann. Phys. 393 (2018) 145–166.
[46] M. Sharif, K. Nazir, Modern Phys. Lett. A 31 (2016) 1650148.
[47] G. Mustafa, et al., Chinese J. Phys. 60 (2019) 362–378.
[48] M.F. Shamir, et al., Chinese J. Phys. 73 (2021) 634.
[49] A. Banerjee, et al., Ann. Phys. 433 (2021) 168575.
[50] G. Mustafa, et al., Chinese J. Phys. 65 (2020) 163.
[51] M. Zubair, et al., Eur. Phys. J. C 77 (2017) 680.
[52] M. Zubair, et al., Internat. J. Modern Phys. D 28 (4) (2019) 1950067.
[53] G. Mustafa, et al., Commun. Theor. Phys. (Beijing) 75 (2023) 095201, 10.
[54] G. Mustafa, et al., Astrophys. J. 941 (170) (2022) 20.
[55] G. Mustafa, et al., Phys. Lett. B 848 (2024) 138407.
[56] N.S. Kavya, et al., Chinese J. Phys. 87 (2024) 751–765.
[57] G. Mustafa, et al., J. High Energy Astrophys. 42 (2024) 1–11.
[58] G. Mustafa1, Zinnat Hassan3, P.K. Sahoo, Classical Quantum Gravity 41 (2024) 235001, 26.
[59] G. Mustafa1, Zinnat Hassan3, P.K. Sahoo, Ann. Physics 437 (2022) 168751.
[60] G. Mustafa, et al., Fortschr. Phys. (2021) 2100048.
[61] G. Alencar, et al., Universe 7 (2021) 238.
[62] G. Cáceres-Aravena, et al., Phys. Rev. Lett. 133 (11) (2024) 116304.
[63] F. Javed, M. Jan, A. Ditta, S. Qaisar, Int. J. Geom. Methods Mod. Phys. 19 (12) (2022) 2250190.
[64] A. Asifa, et al., Int. J. Geom. Methods Mod. Phys. 20 (01) (2023) 2350014.
[65] A. Ashraf, et al., Int. J. Geom. Method Mod. Phys. 21 (12) (2024) 2450208.
[66] M.Z. Gul, et al., Phys. Scr. 99 (2024) 125004.
[67] G. Mustafa, et al., Ann. Phys., Lpz. 536 (9) (2024) 2400155.
[68] S. Tsiopelas, A. Sedrakian, M. Oertel, Eur. Phys. J. A. 60 (6) (2024) 127.
[69] J. Bramante, N. Raj, Phys. Rep. 1052 (2024) 1–48.
[70] M. Bandyopadhyay, R. Biswas, Int. J. Geom. Methods Mod. Phys. 21 (5) (2024) 2450097–2450313.
[71] S.Y. Li, et al., 2023 arXiv preprint arXiv:2308.06768.
[72] J. Song, L.R. Dai, E. Oset, Phys. Rev. D. 108 (11) 114017.
[73] P. Horava, D. Minic, Phys. Rev. Lett. 85 (2000) 1610.
[74] A.Y. Kamenshchik, U. Moschella, V. Pasquier, Phys. Lett. B 511 (2001) 265.
[75] R. Chaubey, A.K. Shukla, Can, J. Phys. 93 (2015) 68.
[76] N. Bilic, G.B. Tupper, R.D. Viollier, Phys. Lett. B 535 (2002) 17.
[77] M.C. Bento, O. Bertolami, A.A. Sen, Phys. Rev. D 66 (2002) 043507.
[78] D. Carturan, F. Finelli, Phys. Rev. D 68 (2003) 103501.
[79] L. Amendola, F. Finelli, C. Burigana, D. Carturan, J. Cosmol. Astropart. Phys. 07 (2003) 005.
[80] R.F. vom Marttens, L. Casarini, W. Zimdahl, W.S. Hipólito-Ricaldi, D.F. Mota, Phys. Dark Univ. 15 (2017) 114.
[81] A. Abdullah, A.A. El-Zant, A. Ellithi, Phys. Rev. D 106 (2022) 083524.
[82] X.-Q. Li, B. Chen, L.-L. Xing, Eur. Phys. J. Plus 135 (2020) 175.
[83] X.-Q. Li, B. Chen, L.-L. Xing, Eur. Phys. J. Plus 137 (2022) 1167.
[84] X.-Q. Li, H.-P. Yan, L.-L. Xing, S.-W. Zhou, Phys. Rev. D 107 (2023) 104055.
[85] A. Aviles, A. Bastarrachea-Almodovar, L. Campuzano, H. Quevedo, Phys. Rev. D 86 (2012) 063508.
[86] V. Sharma, S. Ghosh, Eur. Phys. J. C 81 (2021) 1004.
[87] Shamir, et al., Internat. J. Modern Phys. A 36 (2021) 2150021.
[88] G. Mustafa, et al., Phys. Lett. B 821 (2021) 136612.
[89] S.H. Shekh, et al., Classical Quantum Gravity 40 (5) (2023) 055011.
[90] F. Zwicky, Astrophys. J. 86 (2021) 217, (1937).
[91] F. Rahaman, P.K.F. Kuhfittig, S. Ray, N. Islam, Eur. Phys. J. C 74 (2014) 2750.
[92] K.F. Dialektopoulos, J.L. Said, Z. Oikonomopoulou, Eur. Phys. J. C. 82 (3) (2022) 1–15.
[93] S. Bahamonde, K.F. Dialektopoulos, V. Gakis, J.L. Said, Phys. Rev. D. 101 (8) (2020) 084060.
[94] S. Bahamonde, K.F. Dialektopoulos, J.L. Said, Phys. Rev. D. 100 (6) (2019) 064018.
[95] L.K. Duchaniya, B. Mishra, J.L. Said, Eur. Phys. J. C. 83 (7) (2023) 613.
[96] K.R. Karmarkar, Proc. Indian Acad. Sci. A 27 (1948) 56.
[97] L.P. Eisenhart, Riemannian Geometry Princeton University Press, Princeton, United States of America, 1966.
[98] P. Salucci, A. Burkert, Astrophys. J. 537 (2000) L9.
[99] F. Donato, G. Gentile, P. Salucci, C. Frigerio Martins, M. Wilkinson, G. Gilmore, E. Grebel, A. Koch, R. Wyse, Mon. Not. R. Astron. Soc. 397 (2009) 1169.
[100] J.F. Navarro, C.S. Frenk, S.D.M. White, Astrophys. J. 490 (2) (1997) 493.
[101] K. Jusufi, M. Jamil, P. Salucci, T. Zhu, S. Haroon, Phys. Rev. D 100 (2019) 044012.
[102] Z. Xu, X. Hou, X. Gong, J. Wang, J. Cosmol. Astropart. Phys. 09 (2021) 038.
[103] X. Hou, Z. Xu, M. Zhou, J. Wang, J. Cosmol. Astropart. Phys. 07 (2018) 015.
[104] F. Javed, G. Mustafa, A. Ovgun, M.F. Shamir, Eur. Phys. J. Plus 137 (2022) 1.
[105] F. Javed, S. Mumtaz, G. Mustafa, I. Hussain, L. Wu-Ming, Eur. Phys. J. C 82 (2022) 825.
[106] F. Javed, S. Sadiq, G. Mustafa, I. Hussain, Phys. Scr. 97 (2022) 125010.
[107] G. Mustafa, X. Gao, F. Javed, Fortschr. Phys. 70 (2022) 2200053.
[108] G. Mustafa, et al., Ann. Physics (2023) 169551.
[109] G. Mustafa, et al., Phys. Dark Univ. 45 (2024) 101508.
[110] G. Mustafa, et al., Chinese J. Phys. 88 (2024) 32–54.
[111] S. Sadiq, et al., Chinese J. Phys. 90 (2024) 594–607.